



HAL
open science

The Positive impact of biomineralization for marine corrosion protection of AA5083 alloy

Maria João Marques, J. Jaume, D. Mercier, A. Seyeux, S. Zanna, Régine Basséguy, P. Marcus

► To cite this version:

Maria João Marques, J. Jaume, D. Mercier, A. Seyeux, S. Zanna, et al.. The Positive impact of biomineralization for marine corrosion protection of AA5083 alloy. *Corrosion Science*, 2024, 233, pp.112053. 10.1016/j.corsci.2024.112053 . hal-04732064

HAL Id: hal-04732064

<https://hal.science/hal-04732064v1>

Submitted on 11 Oct 2024

HAL is a multi-disciplinary open access archive for the deposit and dissemination of scientific research documents, whether they are published or not. The documents may come from teaching and research institutions in France or abroad, or from public or private research centers.

L'archive ouverte pluridisciplinaire **HAL**, est destinée au dépôt et à la diffusion de documents scientifiques de niveau recherche, publiés ou non, émanant des établissements d'enseignement et de recherche français ou étrangers, des laboratoires publics ou privés.



Distributed under a Creative Commons Attribution 4.0 International License



The Positive impact of biomineralization for marine corrosion protection of AA5083 alloy

M.J.F. Marques^{a,b,*}, J. Jaume^a, D. Mercier^c, A. Seyeux^c, S. Zanna^{c,**}, R. Basseguy^{a,**}, P. Marcus^c

^a Laboratoire de Génie Chimique, Université de Toulouse, CNRS, INPT, UPS, Toulouse, France

^b Laboratório de Materiais e Revestimentos, LNEG Laboratório Nacional de Energia e Geologia, Lisboa, Portugal

^c Institut de Recherche de Chimie Paris, Research Group Physical Chemistry of Surfaces (IRCP), Chimie ParisTech-CNRS, PSL Research University, Paris, France

ARTICLE INFO

Keywords:

Aluminium alloy
Marine corrosion inhibition
Biomineralization
Extracellular Polymeric Substances (EPS)
MgO and Mg(OH)₂

ABSTRACT

This paper investigates, using surface characterisation techniques (SEM, XPS and ToF-SIMS), the impact of marine biological activity on AA5083 corrosion behaviour during seawater immersion. Different solar exposure (light vs. dark) results in distinct marine fouling development, influencing surface modifications. On the dark side, an Al/Mg oxide/hydroxide layer forms, allowing Cl⁻ penetration. Pitting attack is observed after immersion. For the light side, a dual layer structure forms, with a hydrated Mg rich outer layer, showing barrier effect to Cl⁻ penetration. No localized corrosion occurs. A comparison with abiotic conditions demonstrates the corrosion-inhibiting effect of marine biological activity on AA5083.

1. Introduction

Ensuring the durability of materials should not only be considered relevant from the point of view of minimizing maintenance costs or avoid the occurrence of structural equipment failures. Indeed, increasing the lifetime of materials should also be considered as one of the ways to reduce the impact on the environment, through lower consumption of raw materials and energy for new production.

Given the vast potential of the blue economy and its associated diverse marine activities, new challenges have emerged related to the harshness of the marine environment [1,2]. Simultaneously, concerns about marine pollution and ecological threats posed by conventional corrosion protection technologies have prompted the need for the development of new environmentally friendly corrosion protection solutions [3–6].

In the last decades, new emerging microbial-based technologies have been studied, based on the recognition that microorganisms can influence corrosion behaviour in an advantageous way, the so-called MICI (microbiologically influenced corrosion inhibition), opening different lines of research [4,7–12]. The mechanisms of microbially influenced corrosion inhibition (MICI) are more complex than the mechanisms of the traditional protection strategies but even though the research is still

in the beginning, two main mechanisms have been outlined [3]: direct and indirect inhibition. In the first one, the microorganisms are responsible for the segregation of slow-release inhibitors or surfactants and consume oxygen, which affects the cathodic reaction process. The second one, indirect inhibition mechanism, is associated to the formation of a protective layer on the surface of the material due to metabolic activity of microorganisms. In this context, biomineralization attracted the attention of researchers as a solution to inhibit metal corrosion [13–17].

Biomineralization refers to the processes by which organisms form minerals, so-called biominerals. The term biomineral refers not only to a mineral produced by organisms, but also to the fact that almost all of these mineralized products are composite materials comprised of both mineral and organic components [18–22]. Biomineralization is a widespread phenomenon and has been a large source of inspiration for a variety of fields, ranging from biotechnology, geotechnology, paleobiology to civil engineering and biomedical research [15,23–28]. Comparatively, in the research area of Anticorrosive Coatings, biomineralization has been an underdeveloped approach. Only recently, some scientific publications in the field of corrosion and protection have mentioned the advantage of this MICI mechanism, in which a biogenic mineral precipitation on metal surfaces can form an anticorrosion

* Corresponding author at: Laboratoire de Génie Chimique, Université de Toulouse, CNRS, INPT, UPS, Toulouse, France.

** Corresponding authors.

E-mail addresses: mjoao.marques@lneg.pt (M.J.F. Marques), sandrine.zanna@chimieparitech.psl.eu (S. Zanna), regine.basseguy@toulouse-inp.fr (R. Basseguy).

<https://doi.org/10.1016/j.corsci.2024.112053>

Received 31 January 2024; Received in revised form 11 April 2024; Accepted 12 April 2024

Available online 20 April 2024

0010-938X/© 2024 The Author(s). Published by Elsevier Ltd. This is an open access article under the CC BY license (<http://creativecommons.org/licenses/by/4.0/>).

barrier like a coating [13,17,29–36].

Most of the research were focused on steel and stainless steel, which have been used for many years in marine constructions. However, over recent years, aluminium (Al) has attracted the attention of many industrial sectors linked to seawater [37–39]. Pure Al is relatively soft but alloying it with different elements can induce new properties, such as additional mechanical strength, weldability and corrosion resistance. The aluminium - magnesium alloys (Al - Mg) of the 5XXX series are among the most widely used for marine applications [37,40,41]. In the specific case of the Al-Mg alloy (AA5083), few studies have assessed the influence of biomineralization on its corrosion resistance [42–44] and even less research has been carried out under field conditions [45,46]. Marques et al. [47] performed a field study on corrosion protection for Al built ships, involving a 2-year natural exposure of AA5083 in splash and immersion zones. The results of this Joint Industry Project showed different corrosion behaviour between samples depending on the exposure zones and the biofouling presence. The formation of a compact layer on the Al alloy surface after 2 years of immersion was observed, showing a protective behaviour against corrosion: no severe pitting corrosion attack was detected contrary to the atmospheric/splash exposure. Additionally, complementary experiments revealed that the Al-Mg surface immersed in biotic conditions had a resistance to charge transfer (measured by electrochemical impedance spectroscopy - EIS) at least 2000 times greater than that of the surface exposed in abiotic conditions [48].

In light of this finding and with the vision that the process of biomineralization on a metal surface can be envisaged as an important method in the field of corrosion prevention, the focus of this work is on the chemical and structural characterisation of the surface modifications that occurred on AA5083 during 2 months of immersion in natural seawater. The aim is to make progress in understanding the characteristics and properties of the biomineralization layer formed on the Al-Mg surface which contributes to the corrosion inhibition effect. The characterisation includes analysis techniques such as SEM/EDX, GD-OES, ToF-SIMS and XPS [49]. A comparison with abiotic conditions (surfaces immersed in sterilized seawater) was performed allowing to demonstrate the inhibitory effect induced by marine biological activity on the corrosion of Al-Mg alloy.

2. Materials and methods

2.1. Samples preparation

AA5083-H111 aluminium alloy (Al-Mg) was supplied by the Comptoir Général des Métaux, Cugnaux, France. The elemental chemical composition is given in Table 1. The hot-rolled plates acquired, 1 mm thick, were cut into test samples of (10 × 20) cm. The material was used as received in an initial rough grinding state, with no additional surface preparation given. Before immersion, surface samples were carefully cleaned with water and alcohol and then dried with air.

2.2. Immersion conditions

2.2.1. Field test-Biotic environment

The marine immersion test was carried out on the platform available at the CNR-IAS Genoa Experimental Marine Station (GEMS) (Fig. 1), located within the Port of Genoa, Genoa, Italy [50].

Table 1

Chemical composition of the Al-Mg alloy samples (extracted from supplier certificate).

AA5083 - H111	Chemical composition (wt%)								
	Mg	Mn	Fe	Si	Cr	Cu	Zn	Ti	Al Balance
	4.35	0.50	0.22	0.11	0.067	0.065	0.018	0.016	
Min.	4.00	0.40	—	—	0.050	—	—	—	
Max.	4.90	1.00	0.40	0.40	0.25	0.10	0.25	0.15	

A set of 8 samples of AA5083 alloy were immersed in natural Mediterranean Seawater for 2 months (between 1st September and 2nd November 2020), the samples were positioned vertically with two sides of exposure, light (direct sunlight) and dark side (in the shade). During immersion, the following seawater parameters were daily measured: temperature (average=22.1 ± 2.4 °C; Min= 17.8 °C; Max= 26.5 °C), conductivity (average= 54.0 ± 4 mS/cm; Min= 45.8 mS/cm; Max= 58.1 mS/cm), salinity (average: 37.5 ± 0.9‰; Min= 35‰; Max= 38.3‰) and pH (average: 8.1 ± 0.1; Min= 8.02; Max= 8.21) [51].

2.2.2. Laboratory test-Abiotic environment

The laboratory test was performed at LGC Toulouse in a closed tank containing 6 L of sterilized natural seawater as the liquid medium, where 3 samples of AA5083 alloy were immersed over a period of 2 months (August-September 2022). During the whole test the solution was oxygenated using air diffusers connected to an aquarium pump. The sterilisation of seawater was obtained by carrying out two successive filtrations using 0.22 µm filters (Millipore) in order to ensure that all marine bacteria are removed. The experimental parameters were the following: the temperature of the room was comprised between 20 and 25 °C, the filtered seawater presented a conductivity of 52.9 mS/cm (at 24.4 °C), a salinity of 37.7‰ and a pH of 8.6 (at 24.7 °C).

2.3. Surface and interface characterisation after immersion tests

After 2 months of abiotic immersion test, the AA5083 samples were rinsed with flowing distilled water and dried under atmospheric conditions before proceeding with the characterisation.

For the AA5083 samples subjected to the biotic immersion test, since the objective of this study was not to characterize the biofilm formed on the surface of the Al-Mg alloy during immersion, but rather to assess the surface modifications as a result of microbiological activity, no chemical fixation process was performed. To maintain the integrity of the sample surfaces to be analysed, the cleaning process was carried out without the use of metal scraping tools or chemical pickling solutions. The way found to facilitate removing the biofouling was to do it under a constant smooth flow of water on the surface. At the end of the cleaning procedure, the AA5083 samples were then rinsed with distilled water and air dried under atmospheric conditions, before proceeding with the surface characterisation.

The entire characterisation process of the samples submitted to biotic immersion (light and dark side) was carried out after the surface cleaning procedure (removal of biofouling). The only exception was the observation by digital microscopy, in which the surfaces before cleaning (with biofouling) were also examined.

2.3.1. Digital microscopy

The AA5083 samples used for both abiotic and biotic immersion tests were observed with a DVM6 Leica digital microscope. In this particular observation, the samples subjected to the biotic immersion test were observed before and after the cleaning procedure of the biofouling present on the surfaces.

2.3.2. Scanning electron microscopy (SEM) with energy dispersive X-ray analysis (EDX)

The aluminium alloy samples exposed for 2 months, in abiotic and biotic environments were characterized, surface and cross-section, by

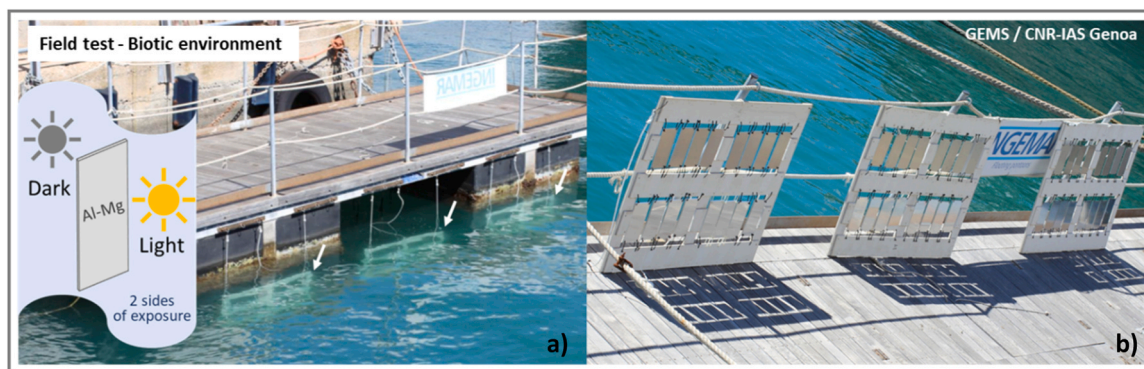


Fig. 1. – Immersion of the Al-Mg samples in natural seawater at the CNR – IAS Genoa experimental marine station (GEMS): (a) Immersion position of the frames (indicated by the arrows) with two different exposure sides, light and dark, and (b) Frames before seawater immersion.

SEM/EDX. The SEM observations were performed using a JSM-7100 F JEOL and a Philips FEG-SEM, mode XL30 microscope coupled with a Pathfinder Thermo Fisher Scientific energy dispersive X-Ray spectrometer (EDX) for elementary chemical analysis.

The cross-section samples were prepared using a cold mounting epoxy resin. Before metallographic preparation, the surface of some samples was previously coated with a fine deposit of platinum, in order to improve the observation process. To reduce charging effects, surface and cross section samples, were coated with a sputtered layer of gold (Au).

SEM characterisation also included an observation after a bending procedure of the samples under study, in order to obtain additional information.

2.3.3. Glow discharge optical emission spectroscopy (GD-OES)

For the GD-OES analyses performed at IRCP in Paris, elemental depth profiles were recorded (GD-PROFILER2, HORIBA Scientific) on AA5083 samples after both immersion tests, abiotic and biotic, respectively.

The radio-frequency (rf) GD-OES analysis was carried out with the following operating conditions: anode (analysed sample) with diameter of 4 mm, argon pressure of 550 Pa, rf power of 40 W and 51,000 Hz.

2.3.4. Time of flight secondary ion mass spectrometry (ToF-SIMS)

For the ToF-SIMS analyses performed at IRCP in Paris, a ToF-SIMS 5 spectrometer (IonToF – Munster Germany) was used, operating at a pressure of around 10^{-9} mbar. Data acquisition and post-processing analysis were performed using the SurfaceLab software v7.2. Analysis was done in high current (HC) bunched mode using Bi^+ primary ions of 25 keV energy at a target current of 1.3 pA over an area of $100 \times 100 \mu\text{m}^2$. Depth profiles were obtained by interlacing analysis with sputtering using a Cs^+ ion gun of 1 keV delivering a 80 nA target current over a $300 \times 300 \mu\text{m}^2$ area. The combined use of Bi^+ primary ions and Cs^+ sputtering ions enabled us to get in-depth analyses of both the organic and inorganic layers. Both ion beams were at an incidence angle of 45° with respect to the sample surface and were well-aligned to ensure analysis at the center of the sputtered crater. Negative secondary ions were recorded.

2.3.5. X-ray photoelectron spectroscopy (XPS)

For the XPS analysis of the surface chemical composition performed at IRCP in Paris, a ThermoElectron ESCALAB 250 Xi spectrometer was used, with a monochromatized Al $K\alpha$ radiation (1486.6 eV). The analyser pass energy was 100 eV for survey spectra and 20 eV for high resolution spectra. The following core level spectra were recorded: Al 2p, Mg 2p, S 2p, P 2p, Cl 2p, O 1s, C 1s, N 1s, Ca 2p. Curve fitting of the spectra was performed with the Thermo Electron software “Avantage”. Binding energies of the component peaks of C 1s and N 1s core levels were corrected with reference to the -CH-CH- binding energy of

285.0 eV.

2.3.5.1. XPS organic compounds characterisation present on Al-Mg surfaces after biotic immersion. Calculations of protein, polysaccharide and oxygenated species molar ratio were performed from data extracted from C 1s and N 1s XPS core levels [52]. The C 1s core level is decomposed in four components attributed to C_1 (C-C, C-H bonds at 285 eV), C_2 (C-O, C-N at 286.6 eV), C_3 (O-C-O; N=C-O at 288.2 eV), associated to the organic matter and C_4 carbonate species at 289.8 eV. The N 1s spectrum is attributed to amide at 400.1 eV.

- C_1 is the molar quantity of carbon bound to carbon and hydrogen. It corresponds to hydrocarbon in lipids and side chains of polysaccharides and proteins and/or carbonaceous contamination.
- C_2 corresponds to the molar quantity of carbon in alcohol (found in polysaccharides including amino sugars and uronic acids) and in amine (found in proteins, amino acids and amino sugars) or amide/peptide bond (found in proteins).
- C_3 is the sum of carbon in N=C-O (peptidic bond) and O-C-O bonds in polysaccharides. C_3 corresponds to carbon in polysaccharides including amino sugars and uronic acids or amide/peptide bond (found in proteins).
- N correspond to the molar quantity of proteins.
- C_{sac} corresponds to molar quantity of carbon in polysaccharides. C_{sac} was calculated by subtracting C-N bonds in proteins to C_2 component ($C_{\text{sac}} = C_2 - N$).
- The molar quantity of carbon involved in the peptidic bond in proteins is $C_{\text{pro}} = C_3 - (1/5) C_{\text{sac}}$. It is known that the atomic ratio C-C-O/O-C-O is 5 in polysaccharides [53,54].
- C_{ox} is associated to other oxygenated species than proteins and polysaccharides i.e. lipids, uronic acids, $C_{\text{ox}} = C_2 + C_3 - C_{\text{pro}} - C_{\text{sac}}$.

2.3.5.2. XPS in-depth analysis surface layers after abiotic and biotic immersion. The Al-Mg in-depth profiling, after 2 months of immersion in abiotic and biotic conditions, was carried out combining a sequence of Argon ion gun etching cycles with XPS analyses. Using an 1 kV ion beam, three etching cycles of 200 seconds each (around 0.2 nm s^{-1}) were performed, reaching a final depth of approximately 100 nm, after a total of 600 seconds of etching.

3. Results

The global visual inspection carried out on all AA5083 samples after the 2 months of immersion in abiotic and biotic environment, respectively, revealed reproducible behaviour for the different replicates tested.

3.1. Digital microscopy

Results of the digital microscope observations performed on AA5083 samples after 2 months of abiotic and biotic immersion are presented in Fig. 2.

For the Al-Mg alloy after abiotic immersion, the surface is covered by a milky white film, with some localized spots, where the presence of superficial deposits is more significant (Fig. 2b).

At the end of the 2 months of biotic immersion, the presence of biofouling is observed (as expected), covering the Al-Mg alloy surface with a different typology according to the exposure side, light or dark (Fig. 2c and d). On the light side of exposure, a presence of so-called soft fouling is identified, consisting of different species of algae (green, brown and red) and a presence of a few calcareous tubes made by tube worms (Fig. 2c). In contrast, on the dark side, much less algae are observed on the aluminium alloy surface, whereas harder fouling, as calcareous fouling organisms, is observed, including tube worms and barnacles (Fig. 2d).

After the biofouling cleaning procedure (Fig. 2e and f), different Al-Mg surface modifications were observed on each side of exposure, light and dark. On the light side, a non-uniform appearance is observed, showing the presence of more dull zones than others and the absence of localized corrosion. In contrast, the dark side exhibits a more pronounced alteration on its surface. This is evident not only through the change in surface colour and the traces of fouling organisms (e.g. tube worms) but also due to the visible pitting attack of the AA5083 surface (indicated by the red circle).

3.2. Scanning electron microscopy (SEM) with energy dispersive X-ray analysis (EDX)

The characterisation by SEM/EDX of the AA5083 samples after the abiotic and biotic immersion tests was performed on surface and cross section. The results are summarized in Figs. 3 and 4.

After 2 months of immersion in abiotic conditions, the Al-Mg alloy reveals, at lower magnification (Fig. 3a), a uniform cracked surface morphology, with no evidence of localized corrosion. At higher magnification (Fig. 3b), a porous surface morphology with a mesh-like

structure is observed. The analysis performed by EDX identified oxygen (O), aluminium (Al) and magnesium (Mg) as the main chemical elements present. Sulphur (S) and carbon (C) were also identified, although with lower intensity.

After biotic immersion, the AA5083 samples exposed to the light side reveal a morphology linked to the previous microbial colonization of the surface. A less uniform morphology and cracked surface is observed with no evidence of localized corrosion (Fig. 3c). A dense needle-shaped morphology is visible at higher magnification (Fig. 3d). The elemental chemical analysis carried out by EDX on distinct zones revealed, in addition to the presence of the same chemical elements detected after abiotic immersion, an enrichment in Mg in some zones.

In contrast, the Al-Mg surfaces exposed on the dark side during biotic immersion (Fig. 3e) showed a cracked surface with a significantly less evident needle-shaped morphology and visible pitting corrosion. The EDX analysis performed near the corrosion pits revealed areas with the metallic substrate exposed (Fig. 3e. spectrum 1) and the presence of some aluminium corrosion products (Fig. 3e. spectrum 2). In the zones without localized corrosion, Mg surface enrichment was not observed, unlike for the Al-Mg surfaces exposed to the light side.

The cross-section characterisation (Fig. 4) allows us to confirm not only the differences between the surface modification of AA5083 after 2 months of abiotic and biotic immersion, but also to verify the differences already observed after biotic immersion, as function of the side of exposure, light or dark.

After 2 months of abiotic immersion (Fig. 4a and b), the Al-Mg alloy shows the formation of a dual-layer structure on the surface, with a compact inner layer homogeneously distributed with an average thickness of 1.1 μm and an outer layer which appears less dense, with a visible lamellar structure perpendicular to the metallic substrate, also homogeneously distributed and with an average thickness of 1 μm . The EDX analysis carried out on both layers, reveals similarities in the chemical elements identified (Al, Mg, O, C and S). The most relevant point to highlight is the enrichment of Mg detected in the outer layer, simultaneously with a lower presence of Al, compared to the inner layer.

The cross section observations of the Al-Mg alloy immersed in biotic conditions confirm one of the differences between the light and dark side of exposure already observed when performing the surface observation:

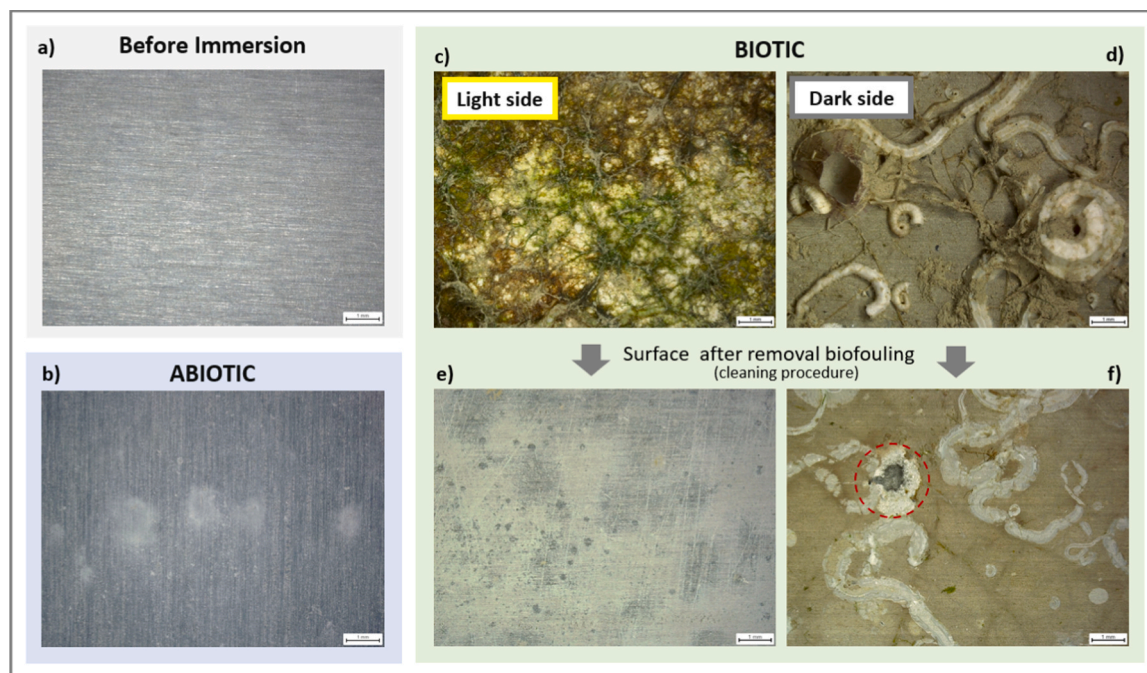


Fig. 2. – Digital microscope observations of Al-Mg samples: (a) before immersion and (b) after 2 months of abiotic immersion and (c/d) after 2 months of biotic immersion, light and dark sides, respectively and (e/f) after biofouling cleaning procedure.

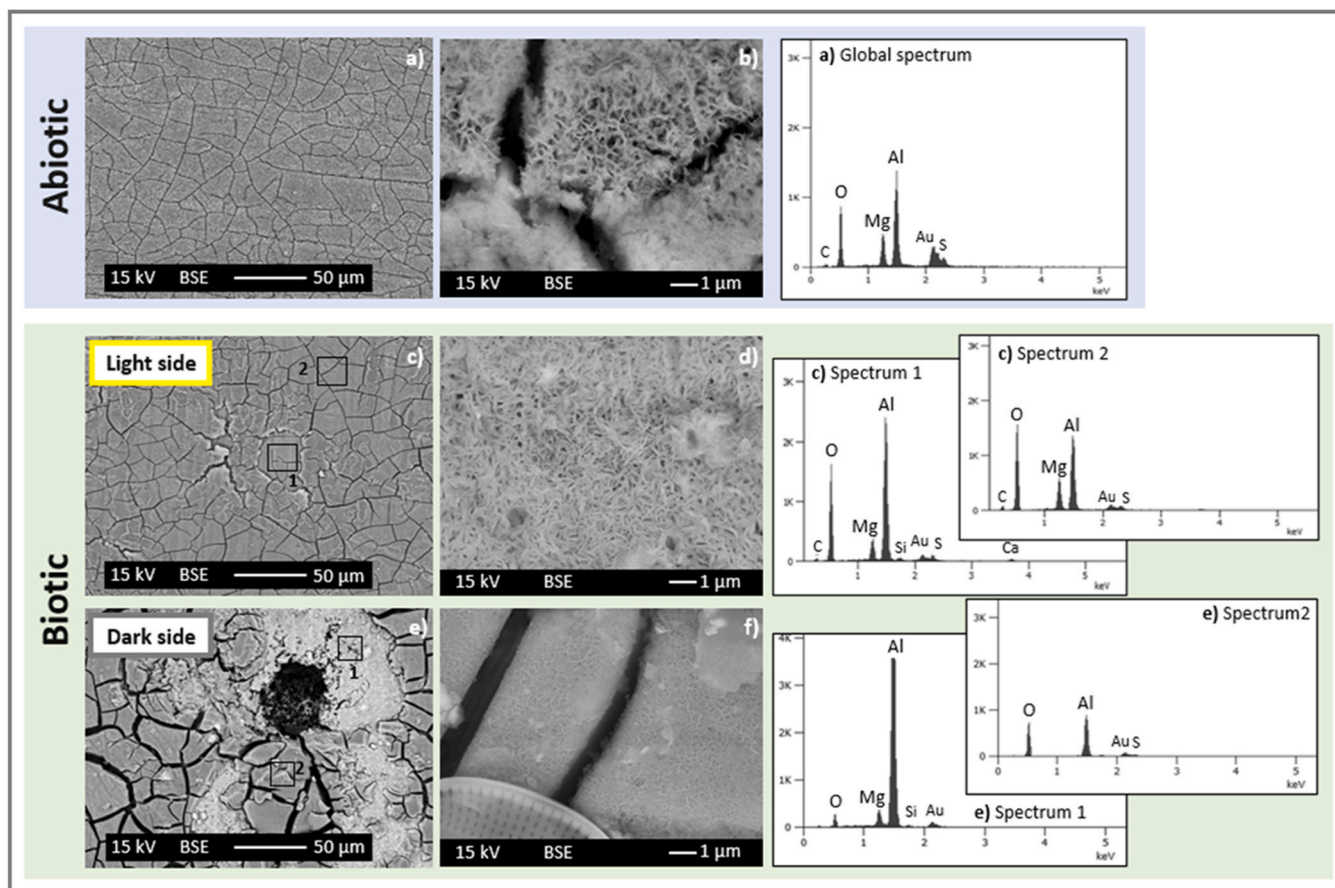


Fig. 3. - SEM/EDX surface characterisation of Al-Mg samples after 2 months of immersion: Abiotic (a/b) and Biotic (Light side of exposure (c /d) & Dark side of exposure (e/f)).

the absence of local attack on the Al-Mg samples exposed to the light side, whereas significant pitting corrosion is observed in some zones of the Al-Mg alloy exposed to the dark side.

For the light side of exposure, the formation of a dual-layer structure on the surface is observed, but not uniformly distributed over the whole surface (Fig. 4c and d). The inner layer, with a compact appearance exhibits an average thickness of 1.8 microns whereas the outer layer, not always visible, shows a very significant heterogeneous distribution with an average thickness of about half a μm . The analysis performed by EDX revealed the qualitative difference in elemental chemical composition between the two layers, inner and outer, the inner layer being richer in aluminium (Al) and the outer layer richer in magnesium (Mg). The presence of calcium (Ca) was also identified in the inner layer, although with a significantly lower amount compared to the other chemical elements detected.

On the dark side, the Al-Mg cross-section observation (Fig. 4e and f), shows the presence of a single layer, with an average thickness of 3.5 μm , heterogeneously distributed. In some zones, a disintegration of the layer is observed, as well as loss of adhesion and, where the layer is no longer present, a localized attack of Al-Mg surface is observed. The EDX results are similar to that obtained for the light side, with an inner layer richer in aluminium (Al). Regarding the presence of magnesium, a lower surface enrichment was observed as compared with the side exposed to light.

In order to complement the SEM surface and cross-section characterisation, an additional observation was undertaken following the application of a bending process to the Al-Mg surfaces after immersion in abiotic and biotic conditions. The objective was to induce the fracture of the layer(s) on the different Al-Mg samples, eliminating metallographic preparation. This approach allowed for a more accurate

observation of the layers structure and morphology (Fig. 5).

After abiotic immersion, the presence of two layers, with distinct morphologies was confirmed. For biotic immersion, the light side exhibits a dual layer structure, each layer showing a characteristic morphology. An inner layer with a compact morphology and an outer layer with a dense lamellar/chip-shaped morphology.

In the case of the Al-Mg samples exposed to the dark side during biotic immersion only one thick inner layer is present, on which, locally, a very thin layer with a porous morphology is observed.

The results are in accordance with those observed in cross-section for both the abiotic and biotic immersion conditions.

3.3. Glow discharge optical emission spectroscopy (GD-OES)

One of the advantages of the GD-OES technique is that it enables, without the requirement of complex sample preparation, to rapidly obtain a depth profile of elemental chemical composition (from a few nm up to several μm), with a detection limit of 0.01%. In this study, the technique proved to be useful in order to confirm the presence of calcium (Ca), detected by EDX, as well to obtain a depth profile for the different layer structure formed on the Al-Mg surfaces, observed by SEM (cross section and bending).

Comparing the obtained profiles (Fig. 6), abiotic and biotic, a difference in sputtering time is observed (shorter time for the Al-Mg alloy immersed under abiotic conditions). This can be related to the immersion conditions of the Al-Mg samples, which in a laboratory (controlled environment/abiotic immersion) is much less complex than in real environment (biotic immersion), leading to a more homogeneous alloy surface. For the Al-Mg alloy exposed to biotic conditions, surfaces are rough, leading to flat GD-OES profiles.

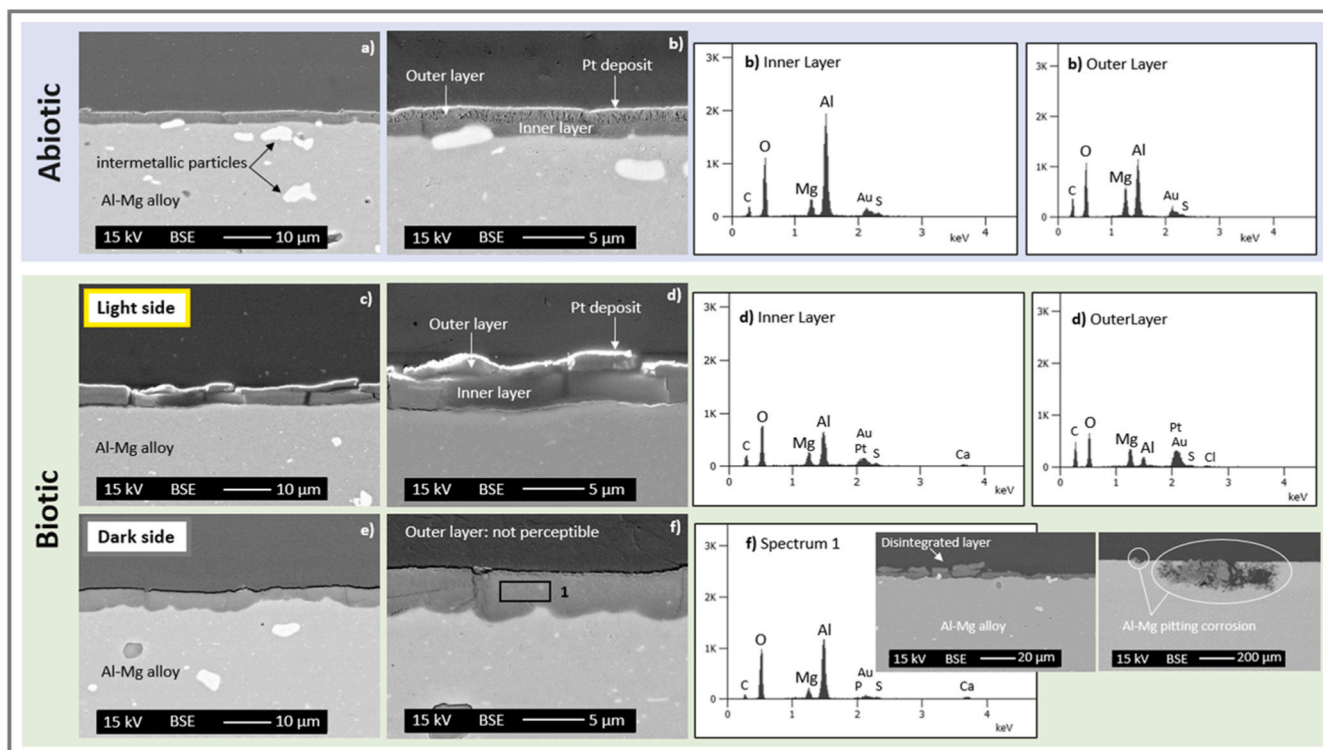


Fig. 4. - SEM/EDX cross-section characterisation of Al-Mg samples after 2 months of immersion: Abiotic (a/b) and Biotic (Light side of exposure (c/d) & Dark side of exposure (e/f)).

In order to facilitate the interpretation of the graphs, only the most relevant chemical elements were included, namely, hydrogen (H), carbon (C), nitrogen (N), oxygen (O), magnesium (Mg), aluminium (Al), and calcium (Ca). The analysis of the results shows that:

- A similar intensity is measured for H, C and O profiles under both abiotic and biotic conditions, in contrast to N, which shows a higher signal in the Al-Mg samples immersed under biotic conditions than under abiotic conditions. This can be associated to the fact that the organic matter in the biotic conditions is composed by carbon and nitrogen compounds as result of organic metabolites produced by living microorganisms on the surface (as bacteria, algae...). Carbon compounds found on the abiotic sample reflect surface carbon contamination.
- The Ca profile for both conditions of immersion, abiotic and biotic (light side and dark side), shows an enrichment in the inner layer. The intensity of Ca signal is similar in all conditions. The plateau is longer for dark side exposure (biotic immersion), which is in line with a thicker inner layer, as observed in the SEM cross-section.
- The Mg profile shows a surface enrichment under both abiotic and biotic conditions, with a higher enrichment in the abiotic case. In this later case (Fig. 6a), the Mg profile clearly showed two distinct zones, one more (outer layer) and one less (inner layer) enriched in Mg, in agreement with the dual structure observed by SEM cross-section.

3.4. Time of flight secondary ion mass spectrometry (ToF-SIMS)

In order to obtain additional information on the different layers formed on the Al-Mg surfaces after 2 months of abiotic and biotic immersion, ToF-SIMS depth profiles were performed (from the surface to a few micrometers). The aim was to combine the high spatial resolution and higher sensitivity of ToF-SIMS to enable a more precise analysis of the composition of the layers.

Fig. 7 presents the ToF-SIMS depth profiles after abiotic and biotic (light and dark side) immersion, for the selected ions MgOH^- , MgO^-

(associated to Mg oxide/hydroxide species), Al_2^- , AlO^- , AlO_2^- (associated to Al oxide/hydroxide species). The ratio between the MgO^- and AlO_2^- ions was plotted to detect the possible enrichment of Mg at the surface. The position of the inner layer / metallic substrate interface is determined from the position where Al_2^- signal reaches its maximum intensity.

For the abiotic case (Fig. 7a) both signals of MgO^- and MgOH^- show an increase at the beginning of the profile followed by a decrease after approximately 6000 seconds of sputtering, after which a second lower intensity plateau is observed, where both MgO^- and MgOH^- signals show similar values. Two distinct zones can clearly be distinguished in the profile. Regarding the AlO^- and AlO_2^- signals, an almost constant intensity is observed until the decay associated with reaching the metallic substrate. The ratio between MgO^- and AlO_2^- clearly show a higher signal in the outer part of the profile as compared to the inner part, confirming the existence of a dual-layer structure, with an outer layer enriched in Mg oxides/hydroxides.

In the case of the Al-Mg samples immersed in biotic conditions (Fig. 7b and c), the ToF-SIMS depth profiles revealed a less sharp metal/inner layer interface, associated to thickness variations of the layers evidenced by SEM observations. Moreover the ToF-SIMS depth profiles revealed differences between the light and dark side of exposure. The surface is characterized by intense MgO^- ; MgOH^- and AlO_2^- signals, indicating that it is mainly formed by Al and Mg oxide and hydroxide. Looking closely at the MgO^- and MgOH^- signals of the Al-Mg surfaces exposed to the light side (Fig. 7b), it can be observed that both show almost the same signal intensity along the whole profile, before reaching the metallic substrate. A drop in the intensity is noticed at the very beginning of the profile, most evident at the first 1600 s of sputtering. After this period of time, the MgO^- and MgOH^- signals revealed to be relatively constant, showing a decay near the interface with the metal substrate. The AlO^- and AlO_2^- signals, showed very similar behaviour to that previously observed for the Al-Mg surface immersed in abiotic conditions.

The $\text{MgO}^-/\text{AlO}_2^-$ ratio enables the identification of two distinct zones. An initial one, indicating a surface enrichment in Mg oxides/hydroxides

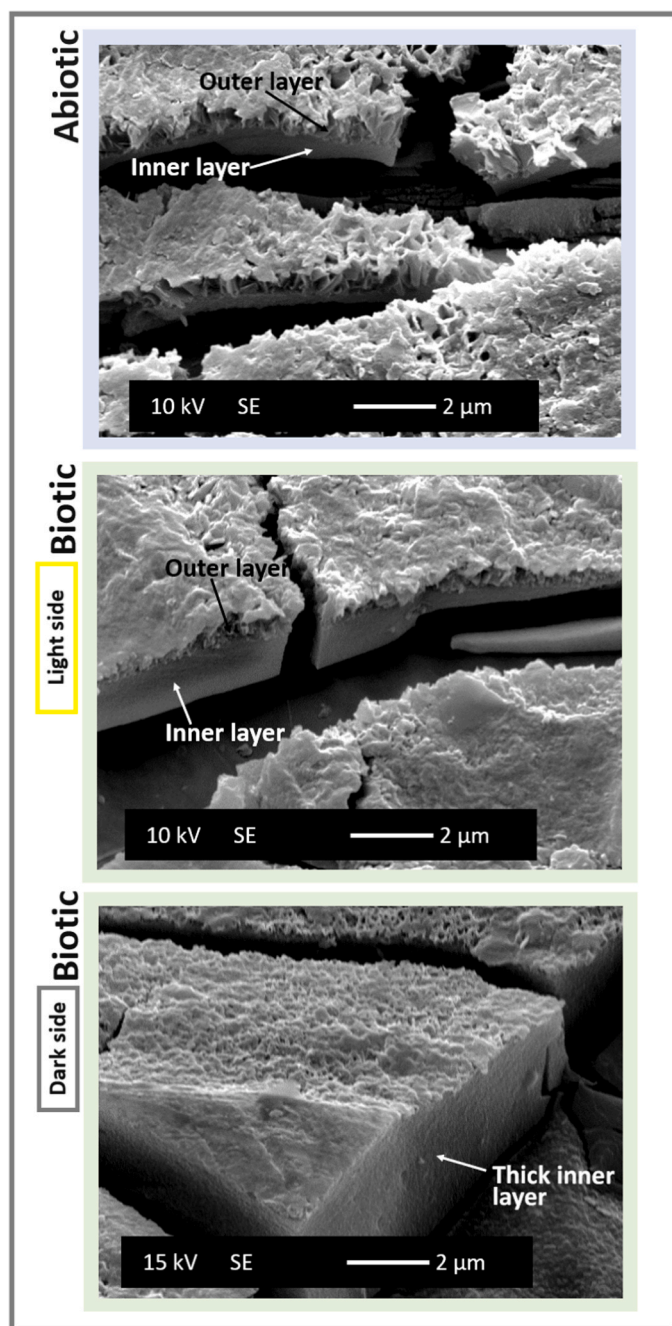


Fig. 5. - SEM observation of Al-Mg surfaces subjected to 2 months of immersion in abiotic and biotic conditions (light and dark side), after a bending process.

which decreases until approximately 1600 s, followed by a second one in which the MgO/AlO_2 ratio signal presents a constant value. Even less significantly than in the abiotic case, the Al-Mg samples exposed to the light side in biotic conditions also reveal a surface modification in the form of a dual-layered structure.

In the case of the Al-Mg surface exposed to the dark side in biotic conditions (Fig. 7c), the surface is also characterized by MgO , MgOH , AlO^- and AlO_2^- signals that have similar profiles in depth.

To discuss the point more precisely, the MgO/AlO_2 ratio is considered. From the ratio, one can observe only a slight enrichment in Mg in the first 200 seconds of sputtering (much less than already observed on the abiotic and biotic light side samples).

In addition to the MgO/AlO_2 ratio, Cl/AlO_2 and SO_4/AlO_2 ratios have been plotted for each substrate on Fig. 8, where the position of the

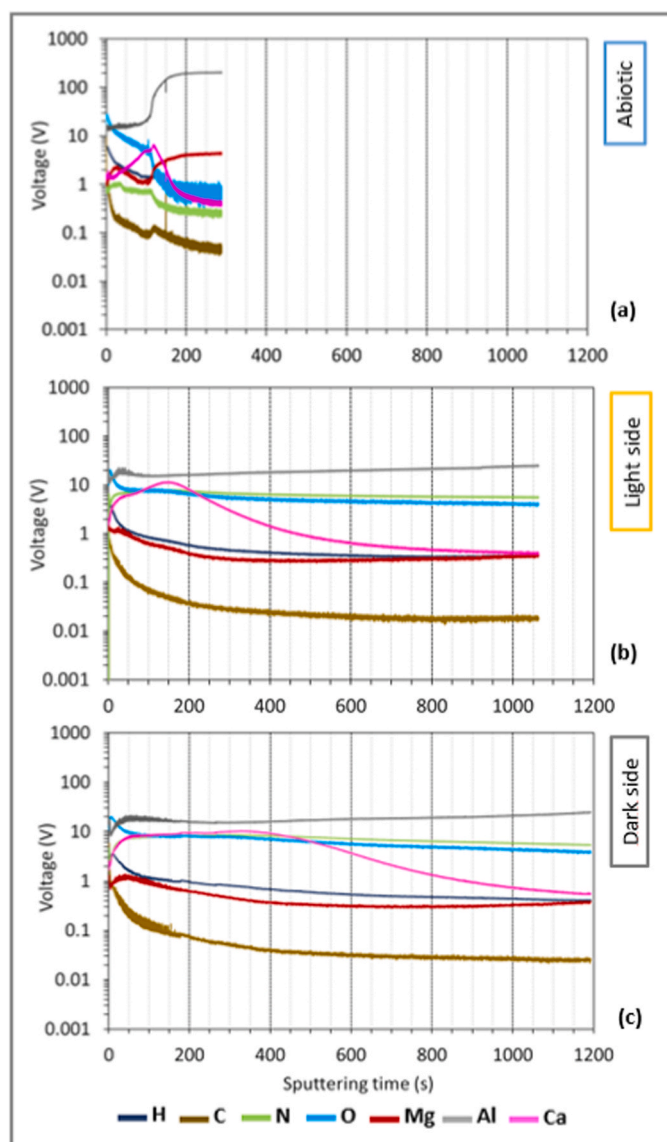


Fig. 6. - GD-OES depth profiles of Al-Mg samples after 2 months of immersion: (a) Abiotic and (b, c) Biotic (light side and dark side of exposure).

metal/inner layer and outer layer/inner layer interfaces are taken from the analysis of the Fig. 7. To better assess the variation of the different ratios in the same scale, the MgO/AlO_2 and SO_4/AlO_2 ratio values were multiplied by 10 and 100, respectively.

The Cl/AlO_2 ratio is used to discuss the chloride penetration into the Al-Mg surface films after the abiotic and biotic immersion. Regarding the Al-Mg surface exposed to the dark side (biotic immersion), the ratio is the highest, showing more penetration of Cl^- (Fig. 8c). Indeed we observe an initial Cl/AlO_2 ratio almost 7 and 2 times higher than that observed for the Al-Mg surfaces exposed to the abiotic (Fig. 8a) and biotic-light side (Fig. 8b) conditions, respectively. Despite the significant initial decrease, to less than 1, the final value remains approximately 4 times higher than that observed in the inner layer of the Al-Mg samples exposed to the abiotic and biotic light side conditions.

For the Al-Mg surface exposed to the light side in biotic conditions (Fig. 8b), the initial Cl/AlO_2 ratio is approximately 4 times higher than that observed on the initial surface of the Al-Mg samples immersed in abiotic conditions. And yet, this ratio decreases in the layer richest in magnesium oxide/hydroxide (outer layer) to reach a final value of approximately 0.1 in the inner layer (less rich in magnesium oxide/hydroxide), a value similar to that observed in the inner layer of the Al-

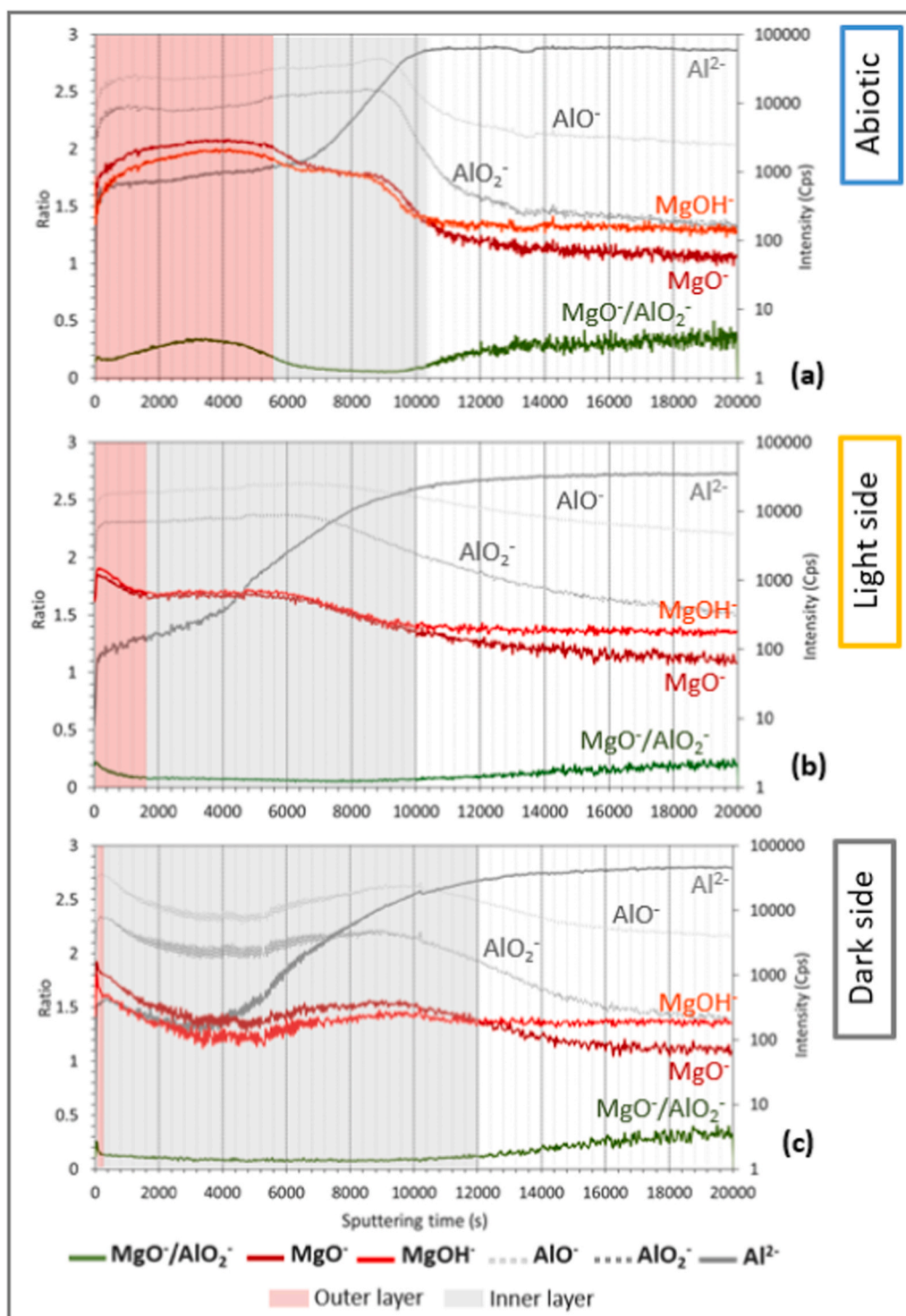


Fig. 7. – ToF-SIMS in-depth profiles (negative ions) and MgO⁻/AlO₂⁻ ratios for Al-Mg alloy surfaces after 2 months of immersion in (a) abiotic conditions, (b) biotic conditions, light side of exposure and (c) biotic conditions, dark side of exposure.

Mg sample immersed in abiotic conditions. Indeed, contrary to the biotic-light side case, the sample exposed to abiotic conditions initially with a lower Cl⁻/AlO₂⁻ ratio (around 0.4) (Fig. 8a), presents only a very slight decrease of the ratio, which remains constant throughout the entire magnesium oxide/hydroxide-rich layer (outer layer) and then shows a slight increase in the inner layer (less rich in magnesium oxide/hydroxide). To conclude, it is clearly shown that the outer layer developed in biotic-light immersion is an efficient barrier to Cl⁻ penetration.

The SO₄⁻/AlO₂⁻ ratios have also been plotted for the three samples to

characterize the presence of sulphate in the outer and/or the inner layer. The Al-Mg surface exposed to the dark side (biotic immersion) presents a value almost 4 and 2 times lower than that initially observed for the Al-Mg surfaces exposed to the abiotic and biotic-light side conditions, respectively. For the Al-Mg sample immersed in abiotic conditions, the SO₄⁻/AlO₂⁻ ratio revealed a value in the outer layer (rich in magnesium oxide/hydroxide) approximately twice as high as that observed for the Al-Mg sample exposed to biotic-light side conditions.

A significant decrease of the ratio can be observed in the inner layer

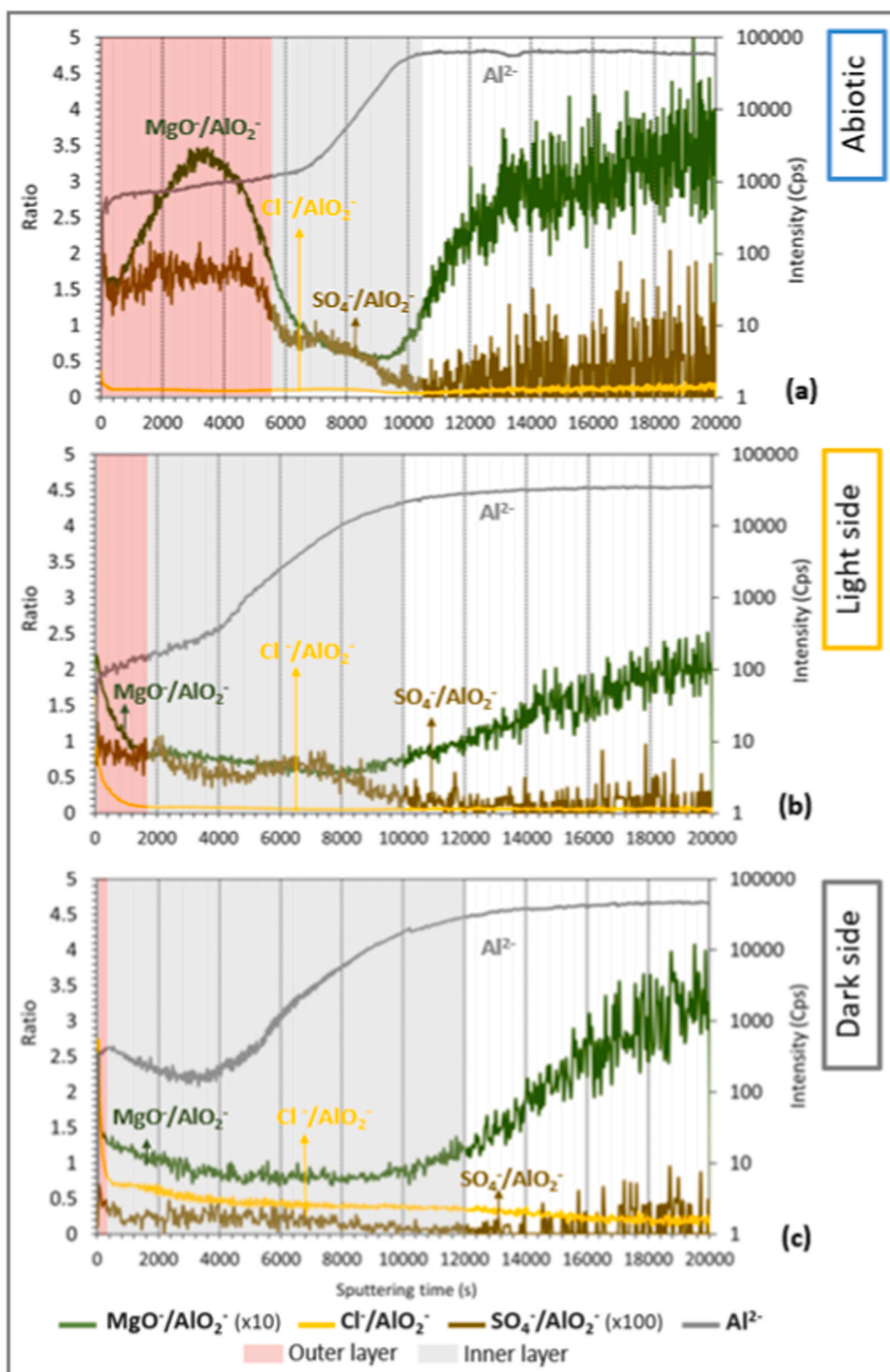


Fig. 8. – ToF-SIMS in-depth profiles (negative ions) for Al-Mg surfaces after 2 months of immersion: $\text{Cl}^-/\text{AlO}_2^-$, $\text{SO}_4^{2-}/\text{AlO}_2^-$ and $\text{MgO}/\text{AlO}_2^-$ ratios under the different immersion conditions: (a) abiotic conditions, (b) biotic conditions, light side of exposure (c) biotic conditions, dark side of exposure.

(showing a value around 0.007). A similar value of the $\text{SO}_4^{2-}/\text{AlO}_2^-$ ratio was also observed in the inner layer of the Al-Mg surface exposed to the light side in biotic conditions. It is interesting to note that the higher the sulphate content in the outer layer, the thicker the outer layer, indicating a possible role of sulphate in the formation mechanism of the outer layer.

3.5. X-ray photoelectron spectroscopy (XPS)

The combination of XPS, with the results already obtained by SEM/EDX, GD-OES and ToF-SIMS, may allow to complement the information regarding the chemical composition of the Al-Mg surface after the immersion in abiotic and biotic conditions.

The capabilities of XPS, a highly surface-sensitive technique, are in this case particularly useful for analysing the organic matter present on Al-Mg surface immersed in biotic conditions (light and dark side) and to perform depth profiling and quantitative analysis (atomic concentrations of the elements present) in the Al alloys surface after immersion in abiotic and biotic conditions.

3.5.1. XPS organic compounds characterisation present on Al-Mg surfaces after biotic immersion

Fig. 9 shows the result of the XPS analysis carried out on the Al-Mg surfaces after immersion in biotic conditions (light and dark sides), with the aim to characterize the presence of organic matter on the extreme surface as a consequence of microbiological activity.

The fitting of the C 1s spectra for both Al-Mg surfaces, light and dark side, after 2 months of biotic immersion (Fig. 9a) reveals, for both cases, four components as described in point 2.3.5.1 of materials and methods section.

The N1s spectra (Fig. 9b) showed only one component for both biotic immersion conditions (399.8 ± 0.1 eV), more intense for the dark side, attributed to amide.

The quantitative analysis based on the fitting results of C 1s and N 1s spectra (Fig. 9c) revealed the presence of more polysaccharides on the light side (44%) compared to the dark side (38%), a similar presence of proteins on both sides of exposure, light (26%) and dark (23%), and more oxygenated species on the dark side (39%) than on the light side (31%). These different functional groups can be attributed to species constituting the extracellular polymeric substance (EPS) secreted by

microorganisms and found outside their cell walls but also to residual presence on the extreme surface of calcareous structures made by tube worms on the dark side (see Fig. 2).

3.5.2. XPS in-depth analysis surface layers after abiotic and biotic immersion

Argon (Ar) sputtering was performed in order to investigate the in-depth composition of the surface layers over about 100 nm (three etching cycles with XPS analysis).

Fig. 10 shows the XPS spectra of the Mg 2p, Al 2p, Mg 2s, Al 2s, S 2p core levels obtained at approximately 100 nm depth for each of the immersed Al-Mg surfaces. Peaks at 74.3 eV and 119.2 eV are associated to Al(III), peaks at 50.4 eV and 90 eV are associated to Mg(II), indicating that the surface is mainly composed of Al and Mg oxides and hydroxides. Although the spectra look similar, it is possible to observe, for the Al-Mg samples that were immersed in abiotic and biotic-light side conditions, the presence of a S 2p peak at high binding energies, 168.3 eV and 167.8 eV, respectively, which are assigned to sulphates. The Al-Mg surface exposed to the dark side during 2 months of biotic immersion did not show the presence of sulphate. The Ca 2p spectra show a peak of low intensity at 348.2 eV for all samples (not shown here), indicating an amount of Ca less than 1% for abiotic and biotic (light and dark sides) immersion. No chloride signal was detected at 200 eV on surfaces analysed by XPS.

Fitting of high-resolution O 1s spectra of the Al-Mg surface immersed 2 months in abiotic and biotic conditions, after 600 seconds of etching (approximate 100 nm depth), are presented in Fig. 11. The spectra

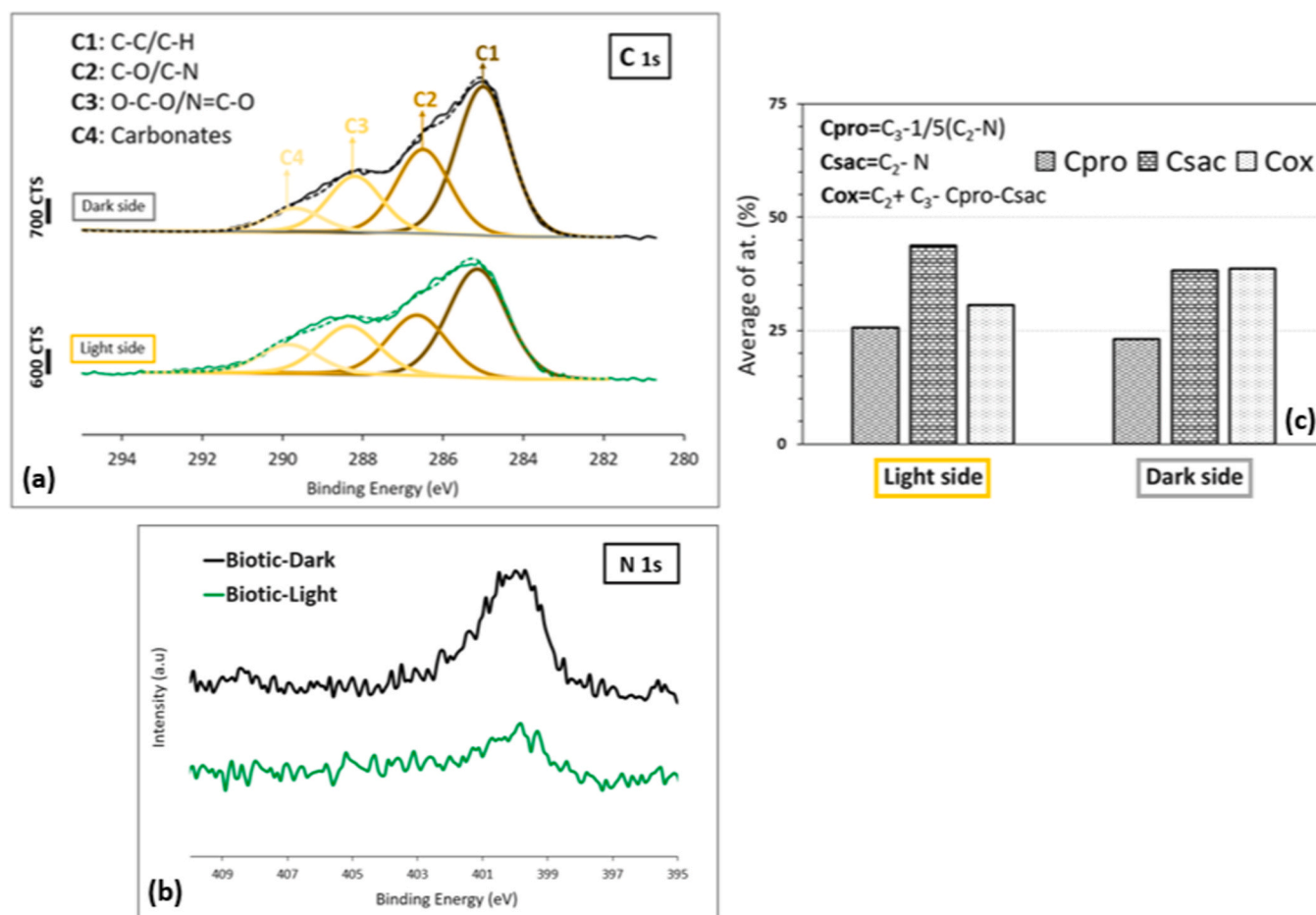


Fig. 9. – (a) XPS spectra of carbon C 1s core level obtained on Al-Mg surfaces after biotic immersion (light and dark sides), (b) XPS spectra of nitrogen N 1s core level obtained on Al-Mg surfaces after biotic immersion and (c) Average of atomic percentage of proteins (Cpro), polysaccharides (Csac) and oxygenated species (Cox) obtained on Al-Mg surfaces exposed to the light and dark sides during the biotic immersion.

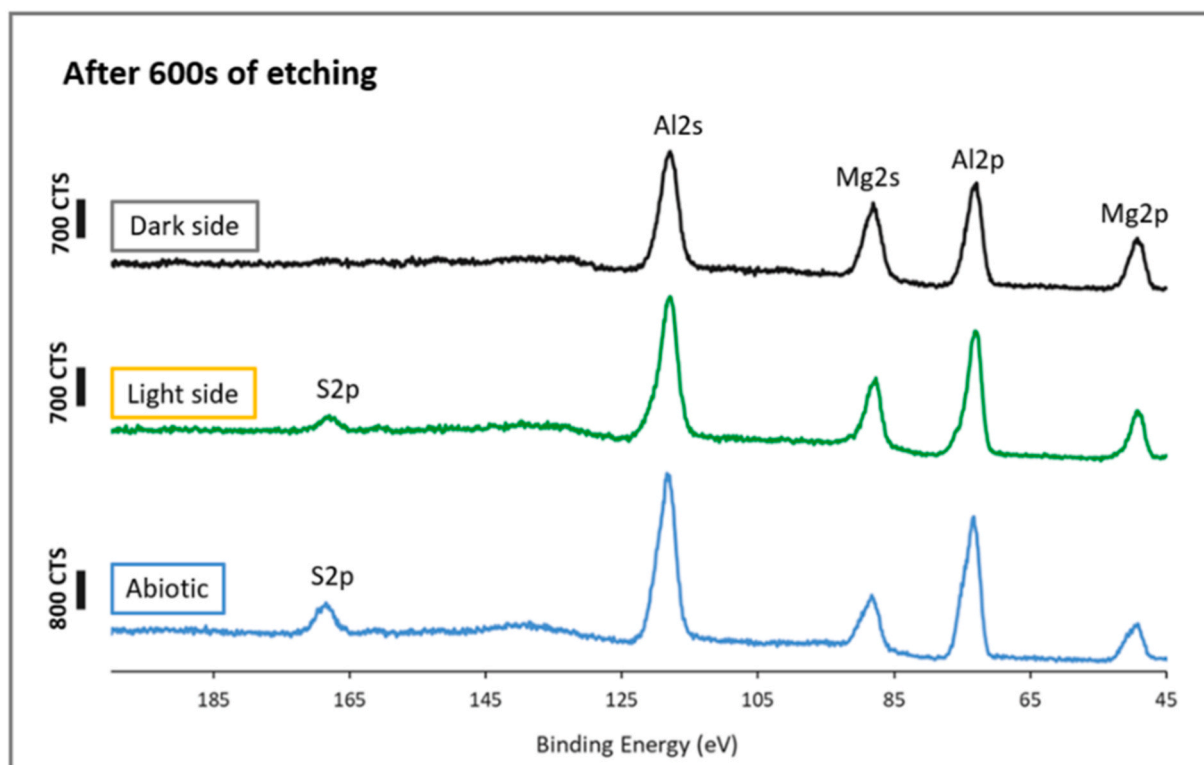


Fig. 10. – XPS spectra obtained after 600 seconds of etching (approximately 100 nm depth) for Al-Mg surfaces after abiotic and biotic (light and dark sides) immersion.

obtained for both immersion conditions show two components at binding energies of 531 eV and 532.8 eV, associated with the presence of oxygen in the form of oxides and hydroxides. However, in the case of the Al-Mg surface immersed in biotic conditions, the spectra clearly show the separation between three different types of oxygen species: oxides, hydroxides and a third component at a binding energy of 535.3 eV assigned to the presence of water, with a significantly higher intensity for surface exposed to the light side than to the dark side.

Fig. 12 shows the atomic concentrations (%) for the three sputtering times, which reflects the changes in composition during the depth profile analysis from the surface to a depth of about 100 nm (600 seconds of sputtering). As the outer layer of the dual structure observed on the Al-Mg surfaces immersed in abiotic and biotic/light side conditions had an average thickness of 1 μm and 0.5 μm , respectively (SEM characterization), it can be assumed that the XPS analysis has been performed in this outer layer. In the case of the Al-Mg surface immersed in biotic/dark conditions, the analysis concerned the external part of the single layer, with an average thickness value of 3.5 μm .

Under biotic conditions, a higher atomic concentration of C than for the abiotic immersion is observed. An organic layer is present under biotic conditions. The higher initial C value, particularly observed in the Al-Mg sample immersed in biotic/dark side, may be associated with the residual presence on the extreme surface of calcareous structures comprised of worm tubes.

After the first sputtering step ($t = 200$ seconds) a relatively constant percentage of atomic concentrations of the different elements/compounds is observed throughout the depth profiles. Regarding the O^{2-} , the Al-Mg surfaces immersed in abiotic conditions show a higher atomic concentration as compared to the biotic conditions. An opposite behaviour was observed for OH^- , showing a higher atomic concentration for the Al-Mg immersed in biotic conditions/light side than in abiotic conditions. Moreover, the results of the XPS depth profiles show the presence of a significantly higher atomic concentration of H_2O on the Al-Mg surface immersed in biotic conditions/light side compared to the

dark side and an absence of it after immersion in abiotic conditions.

As a conclusion, in biotic conditions/light side the outer layer of the dual structure is more hydroxylated and more hydrated than in abiotic conditions.

4. Discussion

Table 2 summarizes major results on the characterisation of the Al-Mg surfaces after 2 months of immersion in seawater, under abiotic and biotic conditions, obtained in this work by surface and interface characterisation techniques. The results are accompanied by a cross-sectional schematic illustration of the Al-Mg surface modifications after the 2 months of immersion in different conditions.

It is noteworthy that after 2 months of immersion in seawater, the only case in which localized corrosion of the Al-Mg alloy was observed was on the surface exposed to the dark side in biotic conditions. That is, the Al-Mg alloy whose surface modification after the immersion period did not reveal the formation of a dual-layer structure.

4.1. Biotic: light vs dark

The different exposure to the solar radiation has resulted in a distinct development of marine fouling on the Al-Mg surfaces. After 2 months of biotic immersion, the light side showed a significant presence of soft-fouling such as noncalcareous algae (green, red and brown) in contrast to the dark side, where hard-fouling, such as barnacles and calcareous tubeworms were mainly observed (see Fig. 2).

The colonization of the metal surface by different micro and macro organisms can influence the corrosion process not only due to the different morphological characteristics of the living organisms involved, but also because of their nature (calcareous or noncalcareous) and the different properties of metabolites produced by them [29,46,55,56].

For both cases, light and dark sides, in the first few minutes and hours of immersion, and in accordance with what has already been

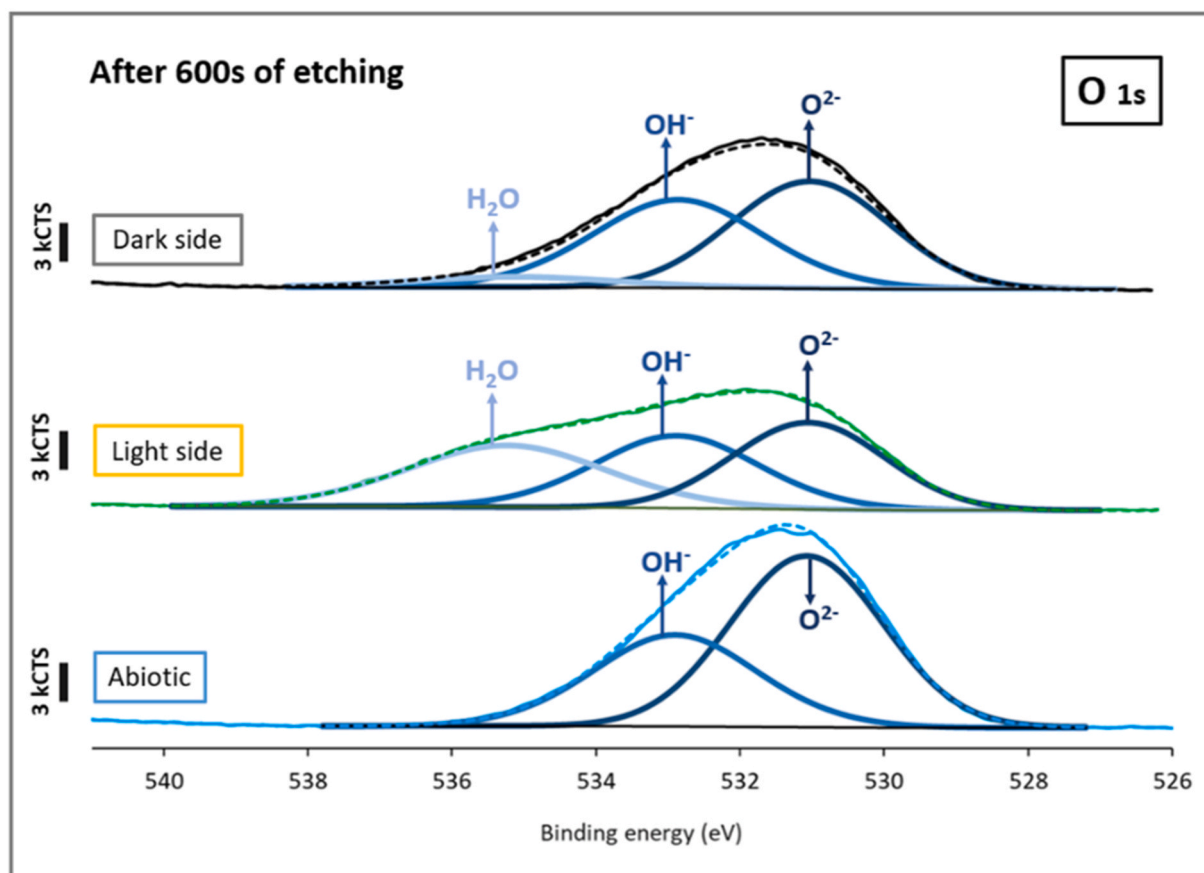


Fig. 11. –XPS spectra of oxygen O 1 s core level obtained for Al-Mg surfaces, after abiotic and biotic (light and dark sides) immersion, after 600 seconds of etching (approximate 100 nm depth).

shown in the literature for different metallic substrates, organic matter naturally dissolved in seawater adsorbs on the surface, followed by the colonization with different types of bacteria [57–61]. It includes photosynthetic bacteria, such as cyanobacteria and phototrophic proteobacteria, which can use light as an energy source for photosynthesis. Their growth and metabolic activities are affected by the light availability and their presence and metabolites consequently influence the type of fouling developed on the metallic surface. XPS analysis performed on both sides of exposure, light and dark (see Fig. 9), revealed differences in the chemical composition of the extracellular polymeric substances (EPS), showing the influence of the different types of fouling. On the light side, the EPS were enriched in polysaccharides in agreement with the marine algae development on the alloy surface. Indeed marine algae (unicellular or colonial microalgae and multicellular marine organisms) are an inexhaustible source of various polysaccharides, including the group of sulphated polysaccharides (SPs) such as carrageenans in red algae, fucoidans in brown algae and ulvans in green algae [62–66]. The presence of sulphate groups, observed in the XPS spectra, is a defining characteristic of these polysaccharides. Sulphate groups are hydrophilic, meaning they have an affinity for water. In line with this characteristic, the XPS depth profile of the Al-Mg surface immersed in biotic conditions/light side showed a significantly higher atomic concentration of H₂O (Fig. 11). When sulphated polysaccharides come into contact with water, these sulphate groups can form hydrogen bonds with water molecules, leading to the absorption and retention of water. This property plays an important role in imparting gel-like consistency to the EPS. Moreover, the presence of divalent cations in the seawater, like Ca²⁺ and Mg²⁺ can help in the multiple cross-linkages between the molecules of different polysaccharide chains. These cross-linkages contribute to the overall stability and consistency of the EPS matrix

[67–70], providing favourable conditions for ions adsorption needed for mineral structure formation.

In contrast, for the dark side, XPS measurements revealed that the concentration in polysaccharides was lower than on the light side, and no sulphates were detected (Figs. 9 and 10). The surface showed a low atomic concentration of H₂O compared to the light side. Hard fouling organisms, such as barnacles and tubeworms, are primarily known for producing extracellular polymeric substances (EPS) rich in proteins and polysaccharides, to attach themselves firmly to the surface, not being typically associated with the production of sulphated polysaccharides [71–73]. Non-sulphated polysaccharides, which lack sulphate groups, may still have some water-absorbing capacity depending on their chemical structure, but it is generally lower than that of sulphated polysaccharides.

SEM characterization revealed that the light side presents a dual layer structure (outer and inner layers). The outer layer has an average thickness of about half a μm and the inner layer (adjacent to the metal substrate) has an average thickness of 1.8 μm . The dark side, in contrast, presents a single thick layer structure, with an average thickness of 3.5 μm . Comparing the two layers at the metal substrate interface, comprising both aluminium oxides, magnesium oxides/hydroxides and calcium, it can be noted that on the dark side the thickness is almost the double.

XPS measurements on Al-Mg surfaces exposed to the light side evidenced an highly hydrated outer layer (see Figs. 11 and 12). On the other hand, the ToF-SIMS analysis also revealed that the diffusion of Cl⁻ ions was reduced in the outer layer (see Fig. 8).

In this context, it can be considered that the outer layer formed on the light side, i.e., the hydrated Mg-rich layer with the presence of sulphated polysaccharides, associated to the biomineralization process,

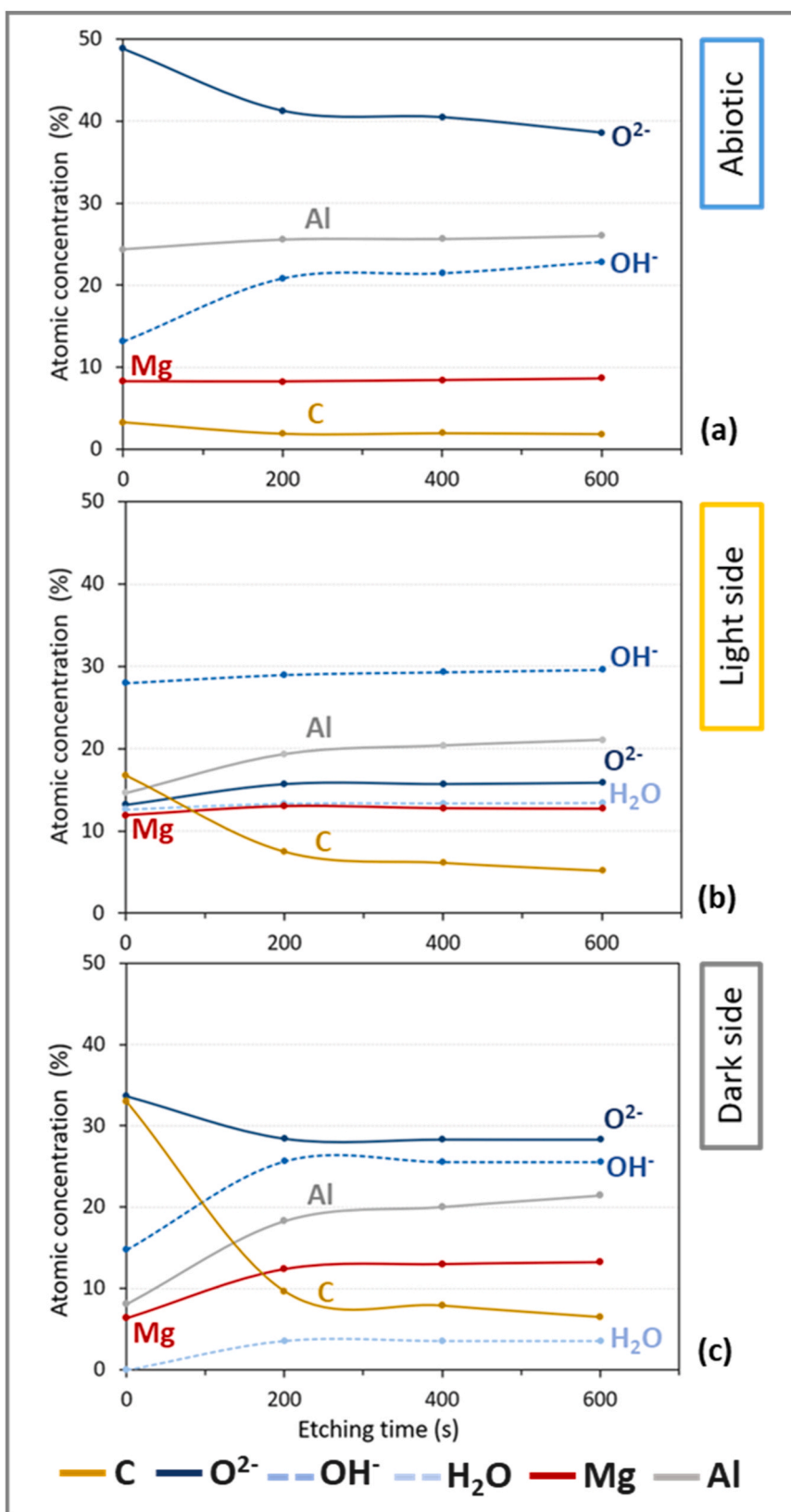
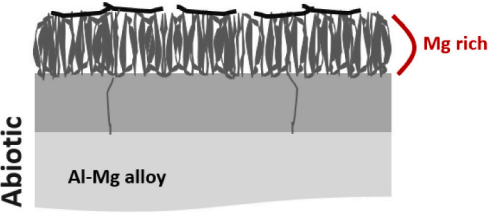
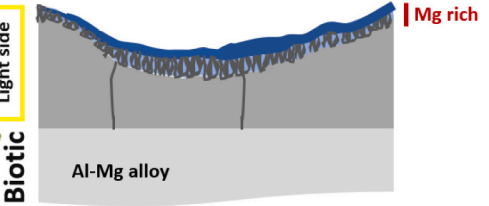
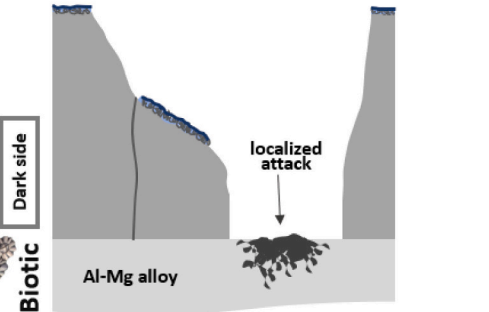


Fig. 12. – XPS depth profile for the Al-Mg samples immersed under the different immersion conditions, after three etch cycles of 200 seconds (approximate 100 nm depth): (a) abiotic conditions, (b) biotic conditions, light side of exposure (c) biotic conditions, dark side of exposure.

Table 2
Summary of the Al-Mg surface characterisation after 2 months of Abiotic and Biotic seawater immersion.

Cross-section scheme	Based on the results of the different characterisation techniques
	<ul style="list-style-type: none"> • Dual layer structure. (homogeneous thickness of outer and inner layer) • Cracked and needle shaped surface morphology. • Presence of sulphate on the surface. • Outer layer: richer in MgO and Mg(OH)₂ • No H₂O detected in the outer layer. • Inner layer: Al and Mg oxides/hydroxides, enriched in Ca. • Low Cl⁻ content at the surface, low Cl⁻ penetration. • No pitting attack of the Al-Mg substrate.
	<ul style="list-style-type: none"> • Dual layer structure. (heterogeneous thickness of outer and inner layer) • Organic matter associated to EPS covering the extreme surface of the outer layer. • Cracked and dense needle shaped surface morphology. • Presence of sulphate on the surface. • Outer layer: richer in MgO and Mg(OH)₂ • High H₂O %at. in the outer layer: hydrated outer layer. • Inner layer: Al and Mg oxides/hydroxides, enriched in Ca. • Higher Cl⁻ content compared to the abiotic surface, low Cl⁻ penetration. • No pitting attack of the Al-Mg substrate.
	<ul style="list-style-type: none"> • Single layer structure (heterogeneous thickness). • Some organic matter associated to EPS and residual presence of calcareous structures on the extreme surface. • Cracked surface morphology. (Significantly less evident needle shaped morphology) • Low enrichment in MgO and Mg(OH)₂ on the top of the layer. • Low amount of H₂O at extreme surface. • Single layer: Al and Mg oxides/hydroxides, enriched in Ca. • Higher Cl⁻ content compared to the abiotic surface, high Cl⁻ penetration. • Localized corrosion. Pitting attack of the Al-Mg substrate.
<div style="display: flex; justify-content: space-around; align-items: center;"> <div style="display: flex; align-items: center;"> <div style="width: 20px; height: 10px; background-color: #0056b3; margin-right: 5px;"></div> EPS (Extracellular polymeric substance) </div> <div style="display: flex; align-items: center;"> Outer layer: richer in MgO and Mg(OH)₂ </div> <div style="display: flex; align-items: center;"> <div style="width: 20px; height: 10px; background-color: #add8e6; margin-right: 5px;"></div> Trapped H₂O </div> <div style="display: flex; align-items: center;"> <div style="width: 20px; height: 10px; background-color: #808080; margin-right: 5px;"></div> Inner layer: Al oxides and Mg oxides/hydroxides, enriched in Ca </div> </div>	

played a role on the inhibition corrosion process of the Al-Mg alloy in biotic conditions: limiting the uniform corrosion (thin inner layer) and preventing the localized corrosion by restricting Cl⁻ ions diffusion. Contrary, on the dark side, the presence of high chloride amount, mainly in the areas where the attack shows to be more intense, explains the pitting corrosion. Obviously, this localized corrosion may be also associated with the effect of galvanic cells formed by different oxygen access

linked to the previous presence of hard fouling on the Al-Mg surface, as described in the literature for steel surfaces [74,75].

4.2. Biotic-light side vs abiotic

The comparison between the Al-Mg surface modifications observed after 2 months of biotic immersion on the light side and abiotic

immersion, allows us to confirm that in both cases a dual-layer structure was formed, with a magnesium-rich outer layer, and no localized corrosion of the substrate.

However, the Al-Mg surface immersed in abiotic conditions having an outer layer thicker and more homogeneously distributed than after biotic-light immersion, did not show a better barrier effect to Cl^- penetration, as shown by ToF-SIMS analyses (see Fig. 8a and b). This behaviour suggests that the outer layer of $\text{Mg}(\text{OH})_2/\text{MgO}$ formed in abiotic and biotic-light side conditions do not have the same properties, which may result from:

- The different density of the surface needle shaped morphology, that was denser on the Al-Mg samples exposed to the biotic/light side than for the abiotic conditions (SEM results, see Figs. 3 and 5). This morphological difference may be influenced by the concentration of sulphate ions. Some publications have reported this influence. Cao et al. have used sulphate ions as additives to control $\text{Mg}(\text{OH})_2$ particle morphology, in a proposed method to synthesize magnesium hydroxide $\text{Mg}(\text{OH})_2$ particles with petal-like morphology [76]. The results indicated that sulphate ions had a great impact on the growth of $\text{Mg}(\text{OH})_2$ particles and changed the crystal morphology of the products. An explanation is that sulphate additives may change the surface characteristics of crystal nucleus, and further affect the growth direction of $\text{Mg}(\text{OH})_2$ crystal grain.
- The chemical composition of the outer layer, specifically the presence of water molecules in the biotic/light, contrary to the abiotic conditions, can impact the penetration of chloride ions. The hydrated outer layer can act as a physical barrier, reducing the diffusion rate of Cl^- towards the metal surface.
- The presence of extracellular polymeric substance (EPS) on the hydrated Mg rich outer layer observed on the biotic/light side surface, may favor adsorption and complexation phenomena. The functional groups of the EPS can form complexes with Cl^- ions reducing their mobility, making more difficult for them to reach the metal.

It is clear that this Mg rich outer layer, observed in both cases (biotic/light side and abiotic conditions), play a role on the corrosion process of the alloy. However, its effect seems conditioned by the nature of the mineralization phenomenon, biotic or abiotic. In the biotic case the presence of marine photosynthetic organisms (algae and micro algae) is responsible for the production of specific extracellular polymeric substance (EPS) and hydration of the Mg-rich outer layer, impacting the corrosion resistance properties of the layer by reducing Cl^- penetration

(see Fig. 13). Indeed, with an initial Cl^-/AlO_2 ratio almost 4 times higher on the extreme surface, the sample exposed to the biotic-light conditions (see Fig. 8b) showed a similar ratio in the inner layer as for that exposed to the abiotic conditions (see Fig. 8c). The thin hydrated outer layer on the biotic light sample limits Cl^- ions penetration.

5. Conclusion

A biotic versus abiotic approach has enabled us to obtain new data on Al-Mg alloy surface modifications during immersion in seawater. It was found that the corrosion process is different for the light and dark sides of exposure in biotic immersion.

On the dark side, where the presence of hard fouling was mainly observed before cleaning, a single thick layer of Al/Mg oxide containing Ca was formed. This layer did not show a barrier effect to Cl^- and pitting of the Al-Mg alloy was observed after two months of seawater immersion. In the case of the light side, where the presence of soft fouling was mainly observed before cleaning, a dual layer structure was formed, in which a hydrated Mg-rich outer layer with extracellular polymeric substances (EPS) on the top has proven to play a role in the corrosion inhibition process as a barrier to the penetration of Cl^- .

The formation of this protective layer on the Al-Mg surface exposed to the light side in biotic conditions is related to the type of fouling developed on the metallic surface. Indeed marine algae, such as red, brown and green algae, are a source of sulphated polysaccharides (SPs), whose hydrophilic properties enhance absorption and retention of water, favouring the formation of the hydrated Mg oxide/hydroxide rich outer layer.

The present work, incorporating a complementary methodology of characterisation techniques, has allowed us to assess the biomineralization process and its role in improving the corrosion resistance of the Al-Mg alloy under biotic conditions. Exploring the potential of marine biological activity/biofouling to create protective layers on metal surfaces can open the way to a novel approach for the development of more environmentally-friendly anticorrosion coatings. The use of biomineralization to inhibit corrosion may become an important method in the field of corrosion prevention.

Declaration of Competing Interest

The authors declare that they have no known competing financial interests or personal relationships that could have appeared to influence the work reported in this paper.

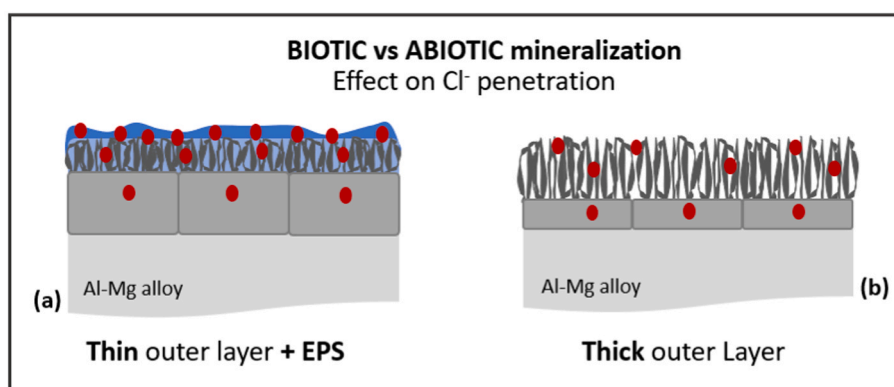


Fig. 13. - Cross-section schematic representation of Cl^- ion penetration through surface layers on Al-Mg after 2 months of immersion in biotic/light side (a) and abiotic (b) conditions. The scheme was designed based on the results of ToF-SIMS and XPS analyses, and SEM observations. *Note: In order to facilitate the schematic representation, a uniform thickness of the outer and inner layers was considered for the biotic case.*

Data Availability

Data will be made available on request.

Acknowledgments

This work was financially supported by the ANR, in the framework of the MICOATEC project (ANR-19-CE08-0018) coordinated by R. Basséguy-LGC.

Région Ile-de-France is acknowledged for partial financial support for the ToF-SIMS equipment.

References

- European Commission. Directorate General for Maritime Affairs and Fisheries., European Commission. Joint Research Centre. The EU blue economy report 2023. [Internet]. LU: Publications Office; 2023 [cited 2023 Oct 11]. Available from: (<https://data.europa.eu/doi/10.2771/7151>).
- M. Abbas, M. Shafiee, An overview of maintenance management strategies for corroded steel structures in extreme marine environments, *Mar. Struct.* 71 (2020) 102718.
- J. Wang, M. Du, G. Li, P. Shi, Research progress on microbiological inhibition of corrosion: a review, *J. Clean. Prod.* 373 (2022) 133658.
- M. Cui, B. Wang, Z. Wang, Nature-inspired strategy for anticorrosion, *Adv. Eng. Mater.* 21 (7) (2019 Jul) 1801379.
- P. Marcus (Ed.), *Corrosion mechanisms in theory and practice*, 3. ed, CRC Press, Boca Raton, 2011, p. 941.
- J.S. George, P. Vijayan P, A.T. Hoang, N. Kalarikkal, P. Nguyen-Tri, S. Thomas, Recent advances in bio-inspired multifunctional coatings for corrosion protection, *Prog. Org. Coat.* 168 (2022) 106858.
- Z. Ahmad, F. Patel, Development of novel corrosion techniques for a green environment, *Int. J. Corros.* 2012 (2012) 1–8.
- K. Alasvand Zarasvand, V.R. Rai, Microorganisms: Induction and inhibition of corrosion in metals, *Int. Biodeterior. Biodegrad.* 87 (2014) 66–74.
- S.K. Karn, A. Bhambri, I.R. Jenkinson, J. Duan, A. Kumar, The roles of biomolecules in corrosion induction and inhibition of corrosion: a possible insight, *Corros. Rev.* 38 (5) (2020) 403–421.
- N. Kip, J.A. van Veen, The dual role of microbes in corrosion, *ISME J.* 9 (3) (2015) 542–551.
- P. Liu, H. Zhang, Y. Fan, D. Xu, Microbially Influenced Corrosion of Steel in Marine Environments: A Review from Mechanisms to Prevention, *Microorganisms* 11 (9) (2023) 2299.
- R. Zuo, Biofilms: strategies for metal corrosion inhibition employing microorganisms, *Appl. Microbiol. Biotechnol.* 76 (6) (2007) 1245–1253.
- N. Guo, Y. Wang, X. Hui, Q. Zhao, Z. Zeng, S. Pan, et al., Marine bacteria inhibit corrosion of steel via synergistic biomineralization, *J. Mater. Sci. Technol.* 66 (2021) 82–90.
- Y. Chen, Y. Feng, J.G. Deveaux, M.A. Masoud, F.S. Chandra, H. Chen, et al., Biomineralization Forming Process and Bio-inspired Nanomaterials for Biomedical Application: A Review, *Minerals* 9 (2) (2019) 68.
- W.M. Kooli, L. Comensoli, J. Maillard, M. Albini, A. Gelb, P. Junier, et al., Bacterial iron reduction and biogenic mineral formation for the stabilisation of corroded iron objects, *Sci. Rep.* 8 (1) (2018) 764.
- A. Arakaki, K. Shimizu, M. Oda, T. Sakamoto, T. Nishimura, T. Kato, Biomineralization-inspired synthesis of functional organic/inorganic hybrid materials: organic molecular control of self-organization of hybrids, *Org. Biomol. Chem.* 13 (4) (2015) 974–989.
- Y. Lou, W. Chang, T. Cui, H. Qian, L. Huang, L. Ma, et al., Microbiologically influenced corrosion inhibition of carbon steel via biomineralization induced by *Shewanella putrefaciens*, *npj Mater. Degrad.* 5 (1) (2021) 59.
- L. Addadi, S. Weiner, Biomineralization: mineral formation by organisms, *Phys. Scr.* 89 (9) (2014) 098003.
- L.A. Estroff, Introduction: Biomineralization, *Chem. Rev.* 108 (11) (2008) 4329–4331.
- P.U.P.A. Gilbert, The organic-mineral interface in biominerals, *Rev. Mineral. Geochem.* 59 (1) (2005) 157–185.
- S. Weiner, An Overview of Biomineralization Processes and the Problem of the Vital Effect, *Rev. Mineral. Geochem.* 54 (1) (2003) 1–29.
- H.C.W. Skinner, H.A. Jahren, Biomineralization. Biomineralization. Treatise on Geochemistry, Elsevier, 2003, pp. 117–184.
- E. Joseph, P. Junier, Metabolic processes applied to endangered metal and wood heritage objects: Call a microbial plumber!, *N. Biotechnol.* 56 (2020) 21–26.
- C.M. Heveran, S.L. Williams, J. Qiu, J. Artier, M.H. Hubler, S.M. Cook, et al., Biomineralization and Successive Regeneration of Engineered Living Building Materials, *Matter* 2 (2) (2020) 481–494.
- Han, Wang, Zhao, Tucker, Zhao, Wu, et al., Mechanism of Biomineralization Induced by *Bacillus subtilis* J2 and Characteristics of the Biominerals, *Minerals* 9 (4) (2019) 218.
- T. Li, Y. Hu, B. Zhang, Biomineralization Induced by *Colletotrichum acutatum*: A Potential Strategy for Cultural Relic Bioprotection, *Front Microbiol* 9 (2018) 1884.
- S. Elsharkawy, A. Mata, Hierarchical Biomineralization: from Nature's Designs to Synthetic Materials for Regenerative Medicine and Dentistry, *Adv. Healthc. Mater.* 7 (18) (2018) 1800178.
- Y. Chen, Y. Feng, J.G. Deveaux, M.A. Masoud, F.S. Chandra, H. Chen, et al., Biomineralization Forming process and bio-inspired nanomaterials for biomedical application: a review, *Minerals* 9 (2) (2019 Jan 23) 68.
- Z. Wang, X. Wang, Y. Huang, H. Zhou, Y. Wu, Y. Sun, et al., Macrofouling organisms: Protection or damage of steel in marine environments? *Corros. Sci.* 212 (2023) 110928.
- Y. Lou, W. Chang, T. Cui, H. Qian, X. Hao, D. Zhang, Microbiologically influenced corrosion inhibition induced by *S. putrefaciens* mineralization under extracellular polymeric substance regulation via *FlrA* and *FlhG* genes, *Corros. Sci.* 221 (2023) 111350.
- X. Hao, Y. Bai, C. Ren, W. Chang, H. Qian, Y. Lou, et al., Self-healing effect of damaged coatings via biomineralization by *Shewanella putrefaciens*, *Corros. Sci.* 196 (2022) 110067.
- Y. Dong, G.L. Song, D. Zheng, Naturally effective inhibition of microbial corrosion by bacterium-alga symbiosis on 304 stainless steel, *J. Clean. Prod.* 356 (2022) 131823.
- L. Comensoli, M. Albini, W. Kooli, J. Maillard, T. Lombardo, P. Junier, et al., Investigation of Biogenic Passivating Layers on Corroded Iron, *Materials* 13 (5) (2020) 1176.
- Z. Guo, S. Pan, T. Liu, Q. Zhao, Y. Wang, N. Guo, et al., *Bacillus subtilis* Inhibits *Vibrio natriegens*-Induced Corrosion via Biomineralization in Seawater, *Front Microbiol* 10 (2019) 1111.
- T. Liu, Z. Guo, Z. Zeng, N. Guo, Y. Lei, T. Liu, et al., Marine Bacteria Provide Lasting Anticorrosion Activity for Steel via Biofilm-Induced Mineralization, *ACS Appl. Mater. Interfaces* 10 (46) (2018) 40317–40327.
- C. Cote, O. Rosas, R. Basséguy, *Geobacter sulfurreducens*: An iron reducing bacterium that can protect carbon steel against corrosion? *Corros. Sci.* 94 (2015) 104–113.
- M.A. Wahid, A.N. Siddiquee, Z.A. Khan, Aluminum alloys in marine construction: characteristics, application, and problems from a fabrication viewpoint, *Mar. Syst. Ocean Technol.* 15 (1) (2020) 70–80.
- Y.J. Yang, S.J. Kim, Electrochemical Characteristics of Aluminum Alloys in Sea Water for Marine Environment, *Acta Phys. Pol. A* 135 (5) (2019) 1005–1011.
- A light durable and economical material for the offshore industry. *Ship & Offshore.* 2013;(6).
- B. Ertuğ, L.C. Kumruoğlu, 5083 type Al-Mg and 6082 type Al-Mg-Si alloys for ship building, *Am. J. Eng. Res.* (2013).
- I. Milošev, B. Kapun, P. Rodić, C. Carrière, D. Mercier, S. Zanna, et al., Mechanism of Corrosion of Cast Aluminum-Silicon Alloys in Seawater. Part 1: Characterization and Field Testing of Bare Alloys in the Adriatic Sea, *Corrosion* 79 (2) (2023) 193–212.
- Y. Gao, D. Feng, M. Moradi, C. Yang, Y. Jin, D. Liu, et al., Inhibiting corrosion of aluminum alloy 5083 through *Vibrio* species biofilm, *Corros. Sci.* 180 (2021) 109188.
- Y. Shen, Y. Dong, Y. Yang, Q. Li, H. Zhu, W. Zhang, et al., Study of pitting corrosion inhibition effect on aluminum alloy in seawater by biomineralized film, *Bioelectrochemistry* 132 (2020 Apr) 107408.
- J. Jaume, M.J.F. Marques, M.L. Délia, R. Basséguy, Surface modification of 5083 aluminum-magnesium induced by marine microorganisms, *Corros. Sci.* 194 (2022 Jan) 109934.
- M.J.F. Marques, A. Benedetti, F. Castelli, M. Delucchi, M. Faimali, S. Delsante, et al., Influence of natural seawater variables on the corrosion behaviour of aluminium-magnesium alloy, *Bioelectrochemistry* 149 (2023) 108321.
- M.J. Marques, J. Jaume, A. Diderot, M.L. Délia, R. Basséguy, Interactions between marine microorganisms and metal: the start point of a new bioinspired solution for corrosion protection, *Mat. ériaux Tech.* 110 (6) (2022) 603.
- M.J.F. Marques, I.N. Alves, R.P. Gonçalves, T.C. Diamantino, AA 5083 Al Alloy Corrosion in Estuarine Environment. Poster presented at; 2013, Eurocorr, Estoril, Portugal, 2013.
- M.J.F. Marques, G. Pavanello, T.C. Diamantino, M. Faimali, R. Basséguy, Influence of microbial activity on Al Alloys in marine medium: natural vs artificial seawater, in: Oral presentation presented at; 2017, 2017, Eurocorr, Prague, Czech Republic, 2017.
- Seyeux A., Zanna S., Marcus P. Surface analysis techniques for investigating biocorrosion. In: *Understanding Biocorrosion* [Internet]. Elsevier; 2014 [cited 2024 Jan 18]. p. 197–212. Available from: (<https://linkinghub.elsevier.com/retrieve/pii/B9781782421207500081>).
- Tomás Prosek, Johan Tidblad. Catalogue of Corrosion Field Exposure Sites in Europe, 1st Edition, European Federation of Corrosion (EFC), 2021.
- A. Montarsolo, R. Stifanese, P. Traverso and V. Piazza. CNRS-LGC Technical Report C1 campaign. 2020 Dec. Report No.: Prot. 4136 04 12 2020.
- P.G. Rouxhet, N. Mozes, P.B. Dengis, Y.F. Dufréne, P.A. Gerin, M.J. Genet, Application of X-ray photoelectron spectroscopy to microorganisms, *Colloids Surf. B: Biointerfaces* 2 (1–3) (1994) 347–369.
- Y. Yang, A.J. Wikiel, L.T. Dall'Agnol, P. Eloy, M.J. Genet, J.J.G. Moura, et al., Proteins dominate in the surface layers formed on materials exposed to extracellular polymeric substances from bacterial cultures, *Biofouling* 32 (1) (2016) 95–108.
- S. Zanna, D. Mercier, E. Gardin, A. Allion-Maurer, P. Marcus, EPS for bacterial anti-adhesive properties investigated on a model metal surface, *Colloids Surf. B: Biointerfaces* 213 (2022) 112413.

- [55] S. Maruthamuthu, M. Eashwar, S.S. Raja, K. Balakrishnan, Effects of microfouling and light/dark regimes on the corrosion potentials of two stainless alloys in seawater, *Biofouling* 7 (4) (1993) 257–265.
- [56] A. Chava, A. Gebruk, G. Kolbasova, A. Krylov, A. Tanurkov, A. Gorbushin, et al., Use of Autonomous Seafloor Equipment for Studies of Biofouling Below the Shallow-Water Zone, *Oceanography* 34 (3) (2021) 61–70.
- [57] P. Vuong, A. McKinley, P. Kaur, Understanding biofouling and contaminant accretion on submerged marine structures, *npj Mater. Degrad.* 7 (1) (2023) 50.
- [58] P.A. Vinagre, T. Simas, E. Cruz, E. Pinori, J. Svenson, Marine biofouling: A European database for the marine renewable energy sector, *JMSE* 8 (7) (2020 Jul 5) 495.
- [59] S.C. Dexter, Role of microfouling organisms in marine corrosion, *Biofouling* 7 (2) (1993 Aug) 97–127.
- [60] M.J. Romeu, F. Mergulhão, Development of antifouling strategies for marine applications, *Microorganisms* 11 (6) (2023) 1568.
- [61] E. Gardin, S. Zanna, A. Seyeux, D. Mercier, A. Allion-Maurer, P. Marcus, Early stage of marine biofilm formation on duplex stainless steel, *Biointerphases* 15 (4) (2020) 041014.
- [62] J. Kang, X. Jia, N. Wang, M. Xiao, S. Song, S. Wu, et al., Insights into the structure-bioactivity relationships of marine sulfated polysaccharides: a review, *Food Hydrocoll.* 123 (2022) 107049.
- [63] J. Muthukumar, R. Chidambaram, S. Sukumaran, Sulfated polysaccharides and its commercial applications in food industries—a review, *J. Food Sci. Technol.* 58 (7) (2021) 2453–2466.
- [64] M. Ciancia, P.V. Fernández, F. Leliaert, Diversity of Sulfated Polysaccharides From Cell Walls of Coenocytic Green Algae and Their Structural Relationships in View of Green Algal Evolution, *Front Plant Sci.* 11 (2020) 554585.
- [65] D. de B. Gurpilhares, T.R. Moreira, J. da L. Bueno, L.P. Cinelli, P.G. Mazzola, A. Pessoa, et al., Algae's sulfated polysaccharides modifications: potential use of microbial enzymes, *Process Biochem.* 51 (8) (2016) 989–998.
- [66] Y. Gao, O.M.E. Schofield, T. Leustek, Characterization of sulfate assimilation in marine algae focusing on the enzyme 5'-adenylylsulfate reductase, *Plant Physiol.* 123 (3) (2000) 1087–1096.
- [67] P.V. Bhaskar, N.B. Bhosle, Microbial extracellular polymeric substances in marine biogeochemical processes, *Curr. Sci.* 88 (1) (2005).
- [68] H.P.S. Abdul Khalil, T.K. Lai, Y.Y. Tye, S. Rizal, E.W.N. Chong, S.W. Yap, et al., A review of extractions of seaweed hydrocolloids: properties and applications, *Express Polym. Lett.* 12 (4) (2018) 296–317.
- [69] J. Lin, G. Jiao, A. Kermanshahi-pour, Algal polysaccharides-based hydrogels: extraction, synthesis, characterization, and applications, *Mar. Drugs* 20 (5) (2022) 306.
- [70] M. Beaumont, R. Tran, G. Vera, D. Niedrist, A. Rousset, R. Pierre, et al., Hydrogel-forming algae polysaccharides: from seaweed to biomedical applications, *Biomacromolecules* 22 (3) (2021) 1027–1052.
- [71] A.K. Halvey, B. Macdonald, A. Dhyani, A. Tuteja, Design of surfaces for controlling hard and soft fouling, *Philos. Trans. R. Soc. A* 377 (2138) (2019) 20180266.
- [72] [cited 2023 Oct 19] T. Harder, L. H. Yee, Bacterial adhesion and marine fouling, *Advances in Marine Antifouling Coatings and Technologies* [Internet] Elsevier 2009 113131 (<https://linkinghub.elsevier.com/retrieve/pii/B9781845693862500053>) [cited 2023 Oct 19].
- [73] [cited 2023 Oct 18] Y. Gu, S. Zhou, Novel Marine Antifouling Coatings: Antifouling Principles and Fabrication Methods, *Wu J. Baghdachi Functional Polymer Coatings* [Internet] 1st ed Wiley 2015 296337 (<https://onlinelibrary.wiley.com/doi/10.1002/9781118883051.ch11>) [cited 2023 Oct 18].
- [74] D.J. Blackwood, C.S. Lim, S.L.M. Teo, X. Hu, J. Pang, Macrofouling induced localized corrosion of stainless steel in Singapore seawater, *Corros. Sci.* 129 (2017) 152–160.
- [75] P. Deng, J. Shanguan, J. Hu, B. Geng, P. Wang, Effect of barnacles on the corrosion behavior of 304 stainless steel, *Metals* 13 (10) (2023) 1649.
- [76] X. Cao, H. Zhao, X. Liu, H.H. Luo, R. Liu, Preparation of petal-like magnesium hydroxide particles by adding sulfate ions, *J. Cryst. Growth* 550 (2020) 125841.